iScience

Article

DNA-PK inhibition sustains the antitumor innate immune response in small cell lung cancer

Graphical abstract

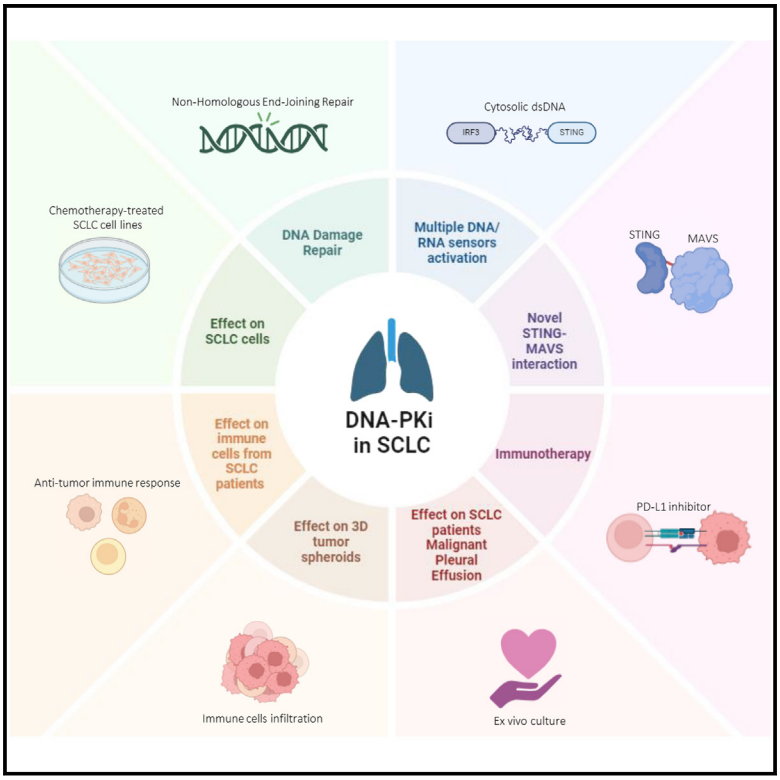

Highlights

- Adding DNA-PKi sequentially after cisplatin boosts the anti-tumor immune response in SCLC
- DNA-PKi enhances innate immunity via the non-canonical STING-MAVS pathway activation
- DNA-PKi and immunotherapy promotes lymphocyte infiltration in tumor spheroids
- Combining DNA-PKi with anti-PD-L1 is a promising maintenance strategy for SCLC patients

Authors

Caterina De Rosa, Floriana Morgillo, Luisa Amato, ..., Lauren Averett Byers, Fortunato Ciardiello, Carminia Maria Della Corte

Correspondence

carminiamaria.dellacorte@unicampania.it

In brief

Molecular biology; Cell biology; Cancer

De Rosa et al., 2025, iScience *28*, 111943
March 21, 2025
https://doi.org/10.1016/j.isci.2025.111943

CellPress

iScience

CellPress
OPEN ACCESS

Article

DNA-PK inhibition sustains the antitumor innate immune response in small cell lung cancer

Caterina De Rosa,[1,11] Floriana Morgillo,[1,11] Luisa Amato,[1] Francesca Iommelli,[2] Viviana De Rosa,[2] Virginia Tirino,[3] Federica Papaccio,[4] Concetta Tuccillo,[1] Gaetano Di Guida,[1] Domenico Michele D'Angiolella,[1] Alessandra Di Liello,[1] Silvia Zappavigna,[1] Michele Caraglia,[1,9] Antonio Gambardella,[1] Valerio Nardone,[5] Kavya Ramkumar,[6] Qi Wang,[7] Jing Wang,[7] Ferdinando De Vita,[1] Davide Ciardiello,[8] Erika Martinelli,[1] Teresa Troiani,[1] Stefania Napolitano,[1] Giulia Martini,[1] Alberto Servetto,[10] Lauren Averett Byers,[6] Fortunato Ciardiello,[1] and Carminia Maria Della Corte[1,12,*]

[1]Department of Precision Medicine, University of Campania Luigi Vanvitelli, 80131 Naples, Italy
[2]Institute of Biostructures and Bioimaging, National Research Council, 80145 Naples, Italy
[3]Department of Experimental Medicine, University of Campania Luigi Vanvitelli, 81100 Caserta, Italy
[4]Department of Medicine, Surgery and Dentistry, "Scuola Medica Salernitana", University of Salerno, 84084 Baronissi, Italy
[5]Radiology and Radiotherapy, Department of Precision Medicine, University of Campania 'Luigi Vanvitelli', 80138 Naples, Italy
[6]Department of Thoracic Head and Neck Medical Oncology, University of Texas MD Anderson Cancer Center, Houston TX 77030, USA
[7]Department of Bioinformatics and Computational Biology, University of Texas MD Anderson Cancer Center, Houston TX 77030, USA
[8]Division of Gastrointestinal Medical Oncology and Neuroendocrine Tumors, European Institute of Oncology (IEO), IRCCS, 20141 Milan, Italy
[9]Laboratory of Precision and Molecular Oncology, Biogem Scarl, Institute of Genetic Research, 83031 Ariano Irpino, Italy
[10]Department of Clinical Medicine and Surgery, University of Naples Federico II, Naples 80131, Italy
[11]These authors contributed equally
[12]Lead contact
*Correspondence: carminiamaria.dellacorte@unicampania.it
https://doi.org/10.1016/j.isci.2025.111943

SUMMARY

Small cell lung cancer (SCLC) is a highly aggressive form of lung cancer with limited treatment options. Patients often respond well to initial chemo-immunotherapy but relapse quickly, necessitating new strategies to enhance immune responsiveness. Recent research explores combining DNA-damaging therapies with immunotherapy to activate the STING pathway and improve the antitumor immune response. The addition of DNA Damage Repair (DDR) inhibitors, such as DNA-PKcs inhibitors, after chemotherapy has shown promise in activating innate immune sensors and enhancing $CD8^+$ T cell and NK cell pathways in SCLC models. This approach could potentially reshape the tumor microenvironment and sustain an antitumor immune response, offering a maintenance strategy for SCLC treatment.

INTRODUCTION

Small cell lung cancer (SCLC) is a challenging malignancy owing to its aggressive biology, characterized by high intrinsic replication stress and DNA damage, and treated for decades only with chemotherapy in the absence of targetable mutations.[1] Currently, four cycles of platinum-based chemotherapy plus an anti-PD-L1 drug, followed by maintenance of the anti-PD-L1 drug until progression, represent the standard of care for patients with extensive-stage (ES) SCLC.[1–3] However, in the absence of clinically validated predictive biomarkers for response to immunotherapy in SCLC, this is still a one-size-fits-all approach, and most patients relapse within a few months after the end of the induction therapy.[4]

According to the recent biological classification of SCLC based on transcriptomic by Gay CM.,[5] SCLC can be divided into four molecular subgroups, three defined by the transcription factors ASCL1 (SCLC-A), NEUROD (SCLC-N), POU2F3 (SCLC-P), and a fourth inflamed subtype (SCLC-I), with specific therapeutic vulnerabilities. SCLC-A cells are sensitive to Bcl2 inhibitors, Myc-high SCLC-N cells are sensitive to AURK inhibitors, SCLC-P cells are sensitive to PARP inhibitors, and SCLC-I cells are sensitive to chemo-immunotherapy and their combinations.[5] More specifically, the SCLC-I subgroup showed high expression of genes related to human lymphocyte antigens (HLAs), immune checkpoints (including *CD274, PDCD1*, *CD38*, *IDO1*, *TIGIT*, VISTA, *ICOS*, and *LAG3*), and stimulator of interferon genes (STING)-induced T cell attracting chemokines, such as CCL5 and CXCL10.[6]

Our group and others have shown that the addition of DNA-damaging therapies (chemotherapy, radiotherapy, or DNA damage repair inhibitors, DDRis) to immunotherapy enhances the antitumor immune response via activation of the canonical STING pathway, which is the major innate immune pathway,[7–9] favoring the recruitment of tumor-infiltrating $CD8^+$ T cells through the secretion of proinflammatory chemokines such as CCL5 and CXCL10.[6,10] However, other roles for STING in regulating these processes remain to be elucidated.

We hypothesized that STING activation may be accompanied by a broader inflammatory response, which occurs physiologically

Table 1. Patients characteristics

Characteristics	Cohort (n = 25)[a,b] Naive	Post-cisplatin	Under chemo-immunotherapy treatment
Age, years; median (range)	64.9 (50–87)	63.2 (48–87)	69.1 (54–84)
Sex, No. (%)			
Female	6 (35.3)	3 (25)	4 (23.5)
Male	11 (64.7)	9 (75)	13 (76.50)
ICI regimen received, No. (%)			
Atezolizumab	–	–	12 (70.6)
Durvalumab	–	–	5 (29.4)

[a]Patients race was White.
[b]Patients Ethnicity was Italian.

in viral infections. Among the innate immune pathways that may be triggered by cytosolic dsDNA and RNA sensors activation induced by anticancer therapies, we investigated the role of IFN-inducible protein 16 (IFI16)[11] and mitochondrial antiviral signaling protein (MAVS)[12] in the activation of the innate immune response. Specifically, in response to RNA-viral infections, oligomeric MAVS is expressed on the outer mitochondrial membrane and induces the activation of the NK-κB and IFN-I signaling pathways.[12]

In this respect, inhibitors of the DDR pathways PARP, Chk1, and Wee-1 are effective in combination with immunotherapy in SCLC via STING.[7,13–15] Among the other DDR proteins, DNA-dependent protein kinase (DNA-PK) is a targetable enzyme involved in non-homologous end-joining (NHEJ)[16–18] and antiviral responses.[19] Most recently, DNA-PK has been identified as a sensor of both a cGAS/STING-dependent and an STING-independent viral DNA sensing pathway.[19,20] We hypothesized that DNA-PK inhibition may modulate multiple innate immune pathways involved in the antitumor immune response in SCLC, similar to its physiological role in antiviral reactions. In the present study, we investigated the effect of targeting DNA-PK in three different SCLC models: cell lines, patient-derived immune cells, 2D/3D cocultures of cancer and immune cells and *ex vivo* SCLC tumor derived from malignant pleural effusion (MPE) of cisplatin-resistant SCLC patient. We showed that DNA-PKi is able to sustain an antitumor immune response by reinforcing the activation of the STING pathway with a non-canonical mechanism, based on interaction with MAVS at the mitochondrial level. These results support DNA-PK as a good target in SCLC, especially in the maintenance of the chemo-immunotherapy response.

RESULTS

Cisplatin increases DDR machinery and multiple DNA/RNA sensors co-activation in SCLC tumors and in SCLC patients-derived PBMCs

Our group previously demonstrated that the expression of STING-related chemokines correlates with features of immune responsiveness in lung cancers and in lung cancer patients-derived peripheral blood mononuclear cells (PBMCs).[21,22] Therefore, we used two models of SCLC (cell lines and patients-derived PBMCs) to assess whether chemotherapy-induced DNA damage may impact DNA/RNA sensors activation. Patients detailed demographic and clinical data are shown in Table 1.

We performed RNA-seq from SCLC cell lines before and after *in vitro* treatment with cisplatin (0.5 μM for 72 h). GSEA revealed that cisplatin treatment induced an enrichment of several DDR-related pathways including DNA repair and E2F targets compared to the control (CTR), thus indicating an upregulation of downstream effectors of the response to DNA damage-induced cellular replication stress. Interestingly, we found an enrichment of innate immune response-related pathways, classified as influenza infection and SARS COV2 translation machinery in the cisplatin-treated SCLC cell lines (Figure 1A; Table S4). DNA sensors are activated in response to both intrinsic and extrinsic DNA damage. Thus, we hypothesized that DDR proteins can mediate innate immune response activation in SCLC cells. We tested the effect of cisplatin treatment (0.5 μM) for 72 h on a panel of SCLC cell lines, such as H82, H446, H661 (Figure 1B), H2141, H524, and H209 (Figure S1A). Western blot analysis revealed an increase in p-H2A.X (widely known as marker of DNA damage) after cisplatin treatment in these cells. Furthermore, we found that cisplatin induced the concomitant activation of DDR proteins, as shown by the upregulation of the levels of the phosphorylated and total forms of DNA-PK, *p*-Chk1 (downstream of ATR) and *p*-Chk2 (downstream of ATM). Importantly, the upregulation of DDR proteins occurred along with an increase in the expression of STING, as well as the cytosolic RNA sensor MAVS, in all the examined cell lines. Moreover, we detected marked chemotherapy-mediated IFI16 upregulation only in two (H82 and H524) of the six SCLC cell lines analyzed. These results indicate that innate immune pathways (mainly STING and MAVS) can be triggered by chemotherapy-induced DNA damage in SCLC models.

To study the effect of the chemotherapy-induced DNA damage on the immune milieu (lymphocytes, NK cells, and macrophages), we used peripheral blood immune cells to test the effect of cisplatin treatment in activating DNA/RNA sensors. We collected blood samples from naive SCLC patients and on the third day of therapy with cisplatin (post-cisplatin patients). First, we investigated the differential gene expression (DEGs) by RNA-seq in SCLC patients-derived PBMCs before and after cisplatin treatment. GSEA analysis showed that cisplatin-treated PBMCs collected from SCLC patients were significantly enriched in antitumor innate immune-related pathways, such as the type I interferons' pathways (IFN-α and IFN-β) and IFN-γ (Figure 1C; Table S4). Interestingly, these gene sets are related to the activation of the DNA/RNA sensors downstream pathways, such as cGAS/STING, MAVS, DDX41, and IFI16.[23–25] Moreover, cisplatin treatment reduced the expression of PD-1 signaling signature in SCLC patients-derived PBMCs, thus indicating that DNA damage-dependent immune cells activation is further enhanced by the antitumor activity of PD-1 gene set downregulation. Then, we investigated the expression of DNA/RNA sensors (STING and MAVS) in PBMCs from naive and post-cisplatin SCLC patients (Figures 1D and S1B). Notably, we found a relevant

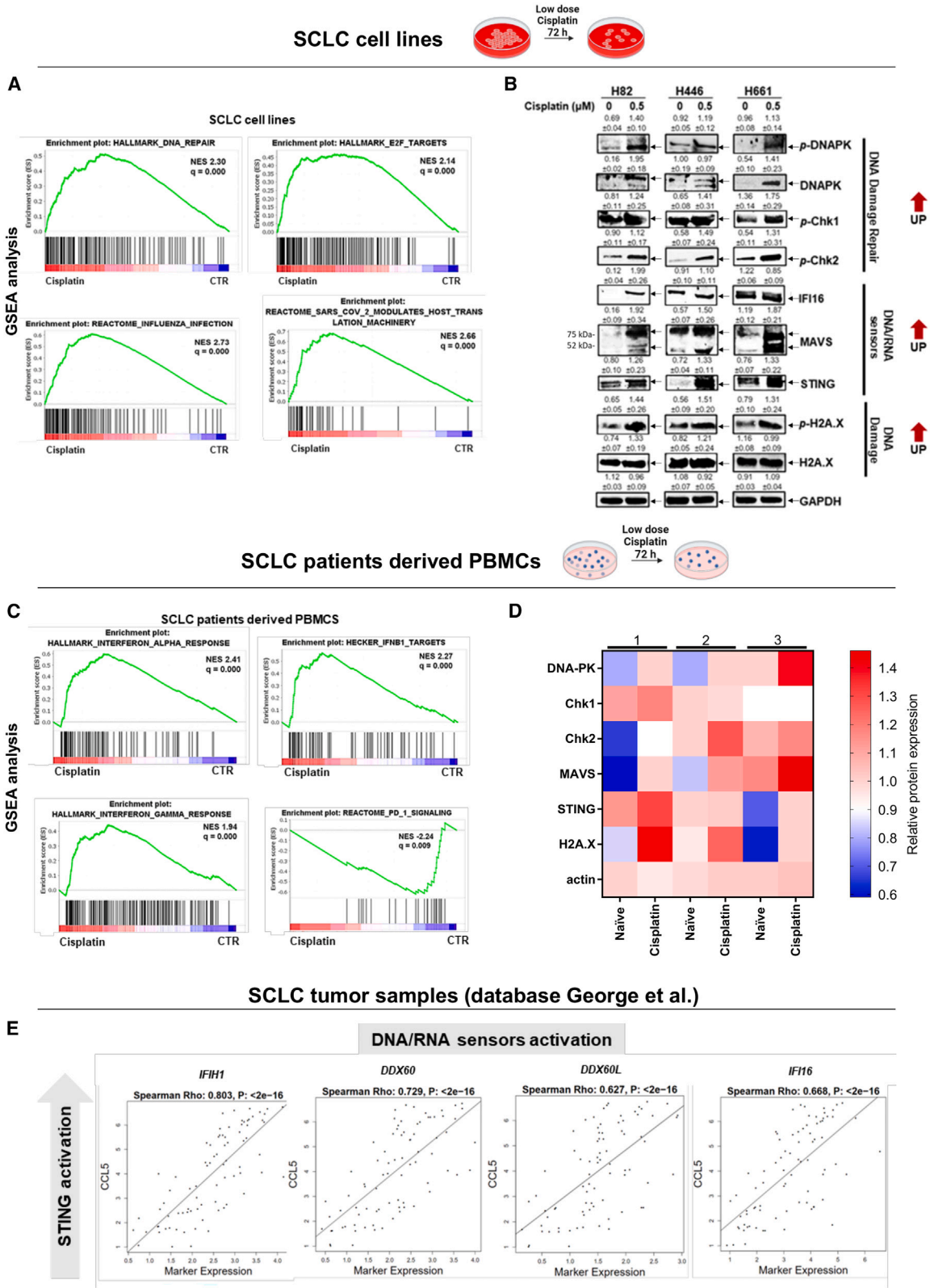

(legend on next page)

upregulation of STING and MAVS in PBMCs collected from SCLC patients' post-cisplatin, thus indicating that in PBMCs as well as in SCLC cells, chemo-immunotherapy triggers DNA damage-related innate immune sensors activation. Therefore, we suggest that the maintenance of intrinsic DNA damage levels in both cancer and immune cells may be a possible mechanism for increasing immune responsiveness of SCLC tumors by activating innate immune pathways.

We afterward explored the expression of additional markers of activated innate immune pathways in tumors tissues from a TGCA database. In particular, we examined the correlation between the gene expression of STING downstream-related chemokine (*CCL5*), a marker of STING pathway activation, and that of other innate immune activators, such as DNA/RNA sensors, in SCLC samples (n = 81) from the cohort of George et al.[26] We found that SCLC tumor tissues with higher STING chemokine levels also exhibited increased expression of genes involved in the activation of *IFITH1* and *DDX60* (Spearman Rho>0.6, p < 0. 001), members of MAVS pathway and *IFI16* (Spearman Rho$\geq$0.6, p < 0.001), a DNA sensor upstream of STING (Figure 1E), demonstrating that different innate immune pathways are simultaneously activated in cancer cells. Taken together, these results suggested that the activation of STING occurs concomitantly with other DNA/RNA sensors expression, in particular MAVS and IFI16.

DNAPK inhibition activates MAVS in PBMC-derived lymphocytes from SCLC patients under treatment with chemo-immunotherapy

In this context, we investigated the effect of different DDR inhibitors on the induction of DNA/RNA innate immune sensors in SCLC patient-derived PBMCs. First, we performed an MTS assay using increasing concentrations of DDR inhibitors (DNA-PKi, ATMi, ATRi, and PARPi) (Figure S2A), to determine the concentrations required to reach 50% of the maximum possible response to treatment (IC_{50}), a sublethal dose, to study the activity of live immune cells. Then, we treated PBMCs collected from SCLC patients with the appropriate IC_{50} of each DDR inhibitor for 72 h. RT-PCR analysis of *STING*, *MAVS*, and *IFI16* mRNA expression revealed that DNA-PKi upregulated both *STING* and *MAVS* more than the other DDR inhibitors (p < 0.0005): ATMi had little impact on *MAVS* upregulation (both p < 0.05), whereas PARPi strongly increased *IFI16* levels (p < 0.0005) (Figure 2A). We also validated the RT-PCR findings by western blot analysis (Figures 2B and S2B).

To deeper investigate the role of chemo-immunotherapy-induced DNA damage in the DNA-PKi-mediated induction of STING/MAVS expression in SCLC immune cells, we serially collected blood samples from treatment-naïve patients with a diagnosis of SCLC (n = 10) and after at least two cycles of chemo-immunotherapy treatment (n = 10). We investigated changes in *STING*, *MAVS*, *cGAS* and *IFI16* mRNA expression in lymphocytes. Briefly, PBMCs were cultured in RPMI supplemented with autologous human serum. After 1 h, monocytes adhered to the plate, while lymphocytes remained in suspension and were separated by collecting the supernatant (Figure S2C). After 24 h, the *in vitro*-expanded T-lymphocytes were treated with 2 μM DNA-PKi and/or ENPP1i for 72 h. We used ENPP1i as a positive control for canonical activation of the STING pathway, being ENPP1 (ecto-nucleotide pyrophosphatase/phosphodiesterase-1) a membrane-bound nucleotide hydrolase identified as the major enzyme that hydrolyzes 2′3′-cGAMP. ENPP1 blockade results in activation of the STING-dependent response.[27]

RT-PCR analysis showed that DNA-PKi increased mRNA levels of *STING*, *MAVS* and *IFI16* in both naive (p < 0.0005) and under treatment (p < 0.0005) SCLC patient-derived lymphocytes. Interestingly, no significant changes in the *cGAS* expression were detected in immune cells derived from naive patients (Figure 2C) or from under treatment SCLC patients (Figure 2D), indicating that DNA-PKi-mediated STING upregulation in immune cells is not strictly dependent on cGAS and may be due to other nucleic acid sensors, suggesting the activation of the non-canonical STING pathway. Indeed, ENPP1i alone was highly effective in upregulating *STING* and *cGAS* expression in naive SCLC patient derived PBMCs. Furthermore, the effect of the combination of DNA-PKi and ENPP1i was most evident at both gene and protein levels in lymphocytes of naive SCLC patients compared to patients under treatment. This specific chemo-immunotherapy-dependent response may provide a rationale for using DNA-PKi in the clinical setting of SCLC patients after specific chemo-immunotherapy administration to maintain high STING levels and prolong the immune-mediated antitumor response. Conversely, the combination of DNA-PKi and ENPP1i may find clinical application in treatment-naïve SCLC patients to sustain antitumor immune system activity.

To better understand the immunomodulatory effects of specific chemo-immunotherapy in SCLC patients-derived PBMCs and to clarify the effect of DNA-PKi on the concomitant activation of nucleic acid sensing and innate immune responses, we

Figure 1. Cisplatin-induced DNA/RNA sensors upregulation in SCLC tumors and in SCLC patients-derived PBMCs

(A) GSEA of cisplatin-treated SCLC cell lines versus CTR. DNA repair and response to viral infections pathways were significantly enriched.

(B) Western blot analysis of DDR and innate immune pathway protein expression in cisplatin-treated SCLC cell lines. GAPDH was used to ensure equal loading. At least three independent experiments were performed. Quantitative analysis of gel bands by morpho-densitometric analysis using ImageJ software. Data are expressed as relative protein levels of each band compared to the corresponding equal loading ±SD. See also Figure S1A and Table S4.

(C) GSEA of cisplatin-treated PBMCs derived from SCLC patients under treatment with chemo-immunotherapy versus CTR, showing significant enrichment of gene sets associated with IFN type I and type II pathways and reduction of PD-1 signaling.

(D) Expression levels of innate immune DNA/RNA sensors in whole PBMC lysates from SCLC patients before and post-cisplatin. β-actin was used to ensure equal loading. At least three independent experiments were performed. Quantitative analysis of gel bands by morpho-densitometric analysis using ImageJ software. Data are expressed as relative protein levels of each band compared to the corresponding equal loading ±SD. See also Figure S1B.

(E) Analysis of gene expression (mRNA levels, scaled as indicated in the axis) revealed a strong correlation between downstream chemokine *CCL5*, a marker of STING pathway activation, and other innate immune pathway activators, such as DNA/RNA sensors (p < 0.001 and Spearman Rho >0.6 for correlation) in SCLC samples from the George et al. dataset (n = 81).

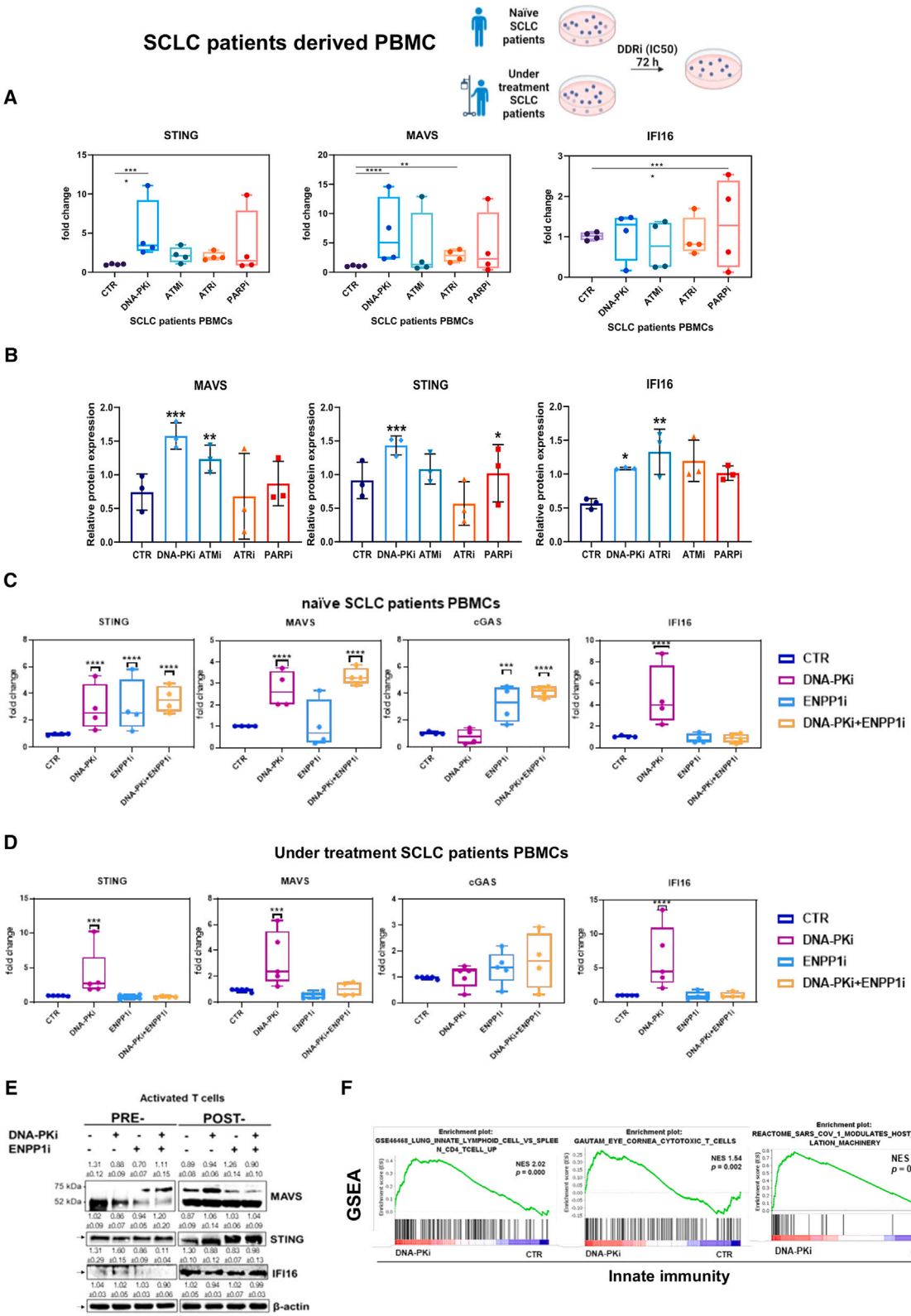

(legend on next page)

performed western blot analysis for STING, MAVS and IFI16 (Figure 2E) of CD3/CD28-activated T lymphocytes collected from naive and under treatment SCLC patients. DNA-PKi preferentially upregulated STING, MAVS, and IFI16, to a greater extent when we collected PBMCs from patients under treatment compared to naive patients. These findings confirmed our hypothesis that immune cells with extensive DNA damage exhibit increased levels of STING and MAVS owing to the synergistic immunomodulatory effect of specific chemotherapy followed by DNA-PKi. In addition, MAVS active fibrillary form (upper band) increased in naive patients upon the combination of DNA-PKi and ENPP1i, while, noteworthy, DNA-PKi alone was the most effective in activating the fibrillary form of MAVS in under treatment SCLC patients. In this regard, 75 kDa MAVS forms large prion-like fibril complexes on the mitochondrial membrane, where it exists in its active form in terms of IFN-I signaling pathway activation.[28,29]

We then investigated the transcriptional changes induced by DNA-PKi via RNA-seq in under treatment SCLC patient-derived PBMCs. The viral infection, lung innate lymphoid cells and cytotoxic T cell datasets were significantly enriched along with impairment of mitochondrial functions in PBMCs from SCLC patients after treatment with DNA-PKi (Figures 2F and S2D; Table S5). These results align with *in vitro* findings and indicate a broad positive pro-immune effect mediated by DNA-PKi after specific chemo-immunotherapy in SCLC patients PBMCs.

In view of the RNA-seq results and given the emerging role of DDR-mediated metabolic changes in immune cells,[30] we explored the effect of DNA-PKi on the metabolism of PBMCs derived from post-chemo-immunotherapy SCLC patients by performing a Seahorse glycolytic rate assay (Figure S2E). We found that DNA-PKi alone or in combination with ENPP1i resulted in a shift to oxidative metabolism, with increased OCR and respiratory reserve. In addition, both DNA-PKi- and ENPP1i-treated immune cells had greater ECARs and glycolytic capacities than CTR cells. This indicates that the increase in oxidative phosphorylation occurred along with increased glycolytic capacity in DNA-PKi-treated immune cells, whereas ENPP1i treatment alone preferentially affected glycolysis rate rather than mitochondrial respiration. Significantly, as indicated by the basal mitoOCR/glycoPER ratio, DNA-PKi treatment alone or in combination with ENPP1i, but not ENPP1i treatment alone, increased acidification rate. These findings indicate that inhibition of DNA-PK in combination with cGAS/STING canonical pathway activation affects both mitochondrial respiration and glycolysis compared to control cells modulating the metabolic fitness of immune cells, which may be beneficial for the maintenance of immune cells activity.

STING-MAVS mitochondrial interaction upon DNA-PK inhibition

Based on these findings, we further aimed to clarify the molecular mechanisms underlying the simultaneous activation of MAVS and STING signaling induced by DNA-PKi in under treatment SCLC patients-derived PBMCs. We analyzed the subcellular localization and physical interaction of STING and MAVS using immunofluorescence (IF) and co-immunoprecipitation (coIP). IF analysis revealed an increase in the mean fluorescence intensity (MFI) of STING and MAVS along with a significant increase of their co-localization in DNA-PKi-treated PBMC-derived immune cells (Figure 3A). $STING_{MFI}$ significantly increased after treatment with DNA-PKi alone (MFI 19.85, $p < 0.0005$), ENPP1i (MFI 17.09, $p < 0.005$) and in combination with ENPP1i (MFI 15.43, $p < 0.005$) compared to the control (MFI 6.30), whereas $MAVS_{MFI}$ significantly increased after treatment with DNA-PKi alone (MFI 14.52, $p < 0.0005$) and in combination with ENPP1i (MFI 12.79, $p < 0.05$) compared to the control (MFI 3.67) and to ENPP1i (MFI 4.88). In Figures S3A and S3B we confirmed the mitochondrial subcellular localization of MAVS. Therefore, the increase of STING-MAVS co-localization upon DNA-PKi treatment, but not in ENPP1i, clearly indicated that DNA-PK inhibition triggers STING upregulation and its translocation to the mitochondrial compartment to interact with MAVS. We hypothesized that the mitochondrial localization of STING may be related to its non-canonical activation mediated by DNA-PKi.

Therefore, in order to assess whether mitochondrial STING may serve as a co-adaptor for MAVS signaling, we performed an IP assay in PBMCs derived from naive and post-cisplatin SCLC patients and then treated them with DNA-PKi and/or ENPP1i (Figure 3C). We found that MAVS and STING physically interacted in DNA-PKi PBMC-derived lymphocytes from both naive and under treatment SCLC patients. It is interesting to note that the interaction between STING and the active fibrillar

Figure 2. DNA-PK inhibition preferentially activates STING and MAVS in PBMCs derived from SCLC patients

(A) RT-PCR analysis of *in vitro* STING, MAVS and IFI16 mRNA expression in PBMC samples isolated from under treatment SCLC patients and cultured with or without 2 μM DDR inhibitors (DNA-PKi, ATMi, ATRi, PARPi) for 72 h. Normalized expression data are presented as the mean ± S.E.M. derived from $n = 3$ technical calculations via the comparative method $2^{-}(\Delta\Delta Ct)$ (reference gene 18S). One-tailed unpaired Student's t test with CI = 95%, ****$p < 0.0005$, ***$p < 0.005$, **$p < 0.05$.

(B) Normalized protein expression quantification of western blot of STING, MAVS and IFI16 in SCLC patients-derived PBMCs with or without DDR inhibitors (2 μM).

(C and D) RT PCR of lymphocyte samples obtained from the PBMCs of naive (A) or under treatment (B) SCLC donors ($n = 10$), cultured in complete media supplemented with 10% human serum for 24 h and then treated with 2 μM DNA-PKi or/and 2 μM ENPP1i for 72 h. Normalized expression data are presented as the means ± S.E.M. derived from $n = 3$ technical calculations via the comparative method $2^{-}(\Delta\Delta Ct)$ (reference gene 18S). One-tailed unpaired Student's t test with CI = 95%, ****$p < 0.0005$, ***$p < 0.005$, **$p < 0.05$.

(E) Western blot analysis of PBMC-derived lymphocytes cultured with T cell activator CD3/CD28 beads before treatment with DNA-PKi or/and ENPP1i for 72 h. Naive SCLC patients did not receive chemo-immunotherapy; under treatment SCLC patients received therapy on the day of blood collection. β-actin was used to ensure equal loading. At least three independent experiments were performed. Quantitative analysis of gel bands by morphodensitometric analysis using ImageJ software. Data are expressed as relative protein levels of each band compared to the corresponding equal loading ±SD.

(F) GSEA of RNA-seq data for SCLC patients-derived PBMCs treated with DNA-PKi versus untreated CTR. See also Figure S2 and Table S5.

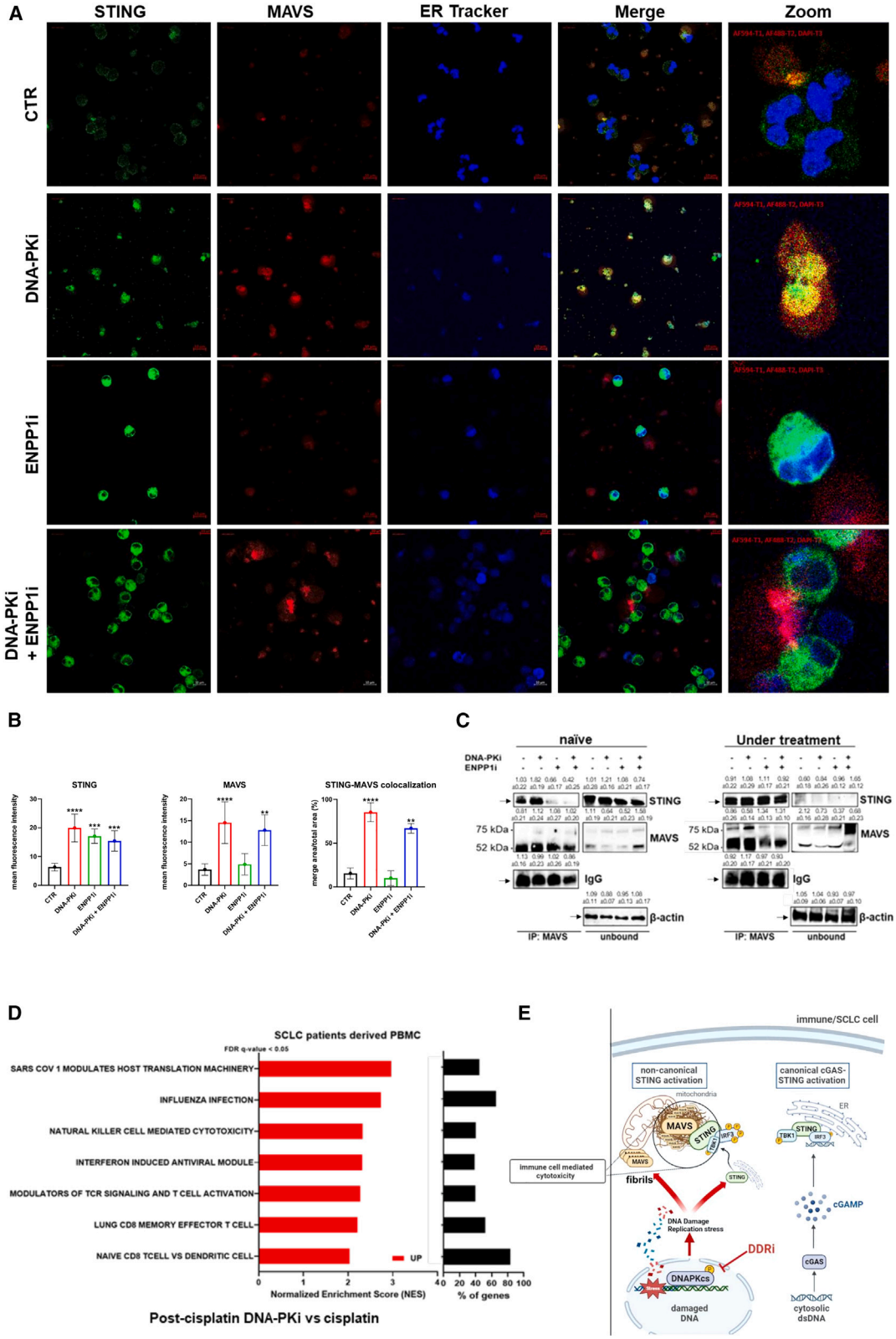

(legend on next page)

form of MAVS (75 kDa band) occurs only in PBMC collected post-cisplatin and after DNA-PK inhibition. In contrast, ENPP1i did not induce STING translocation to the mitochondria nor the formation of a complex with MAVS. To assess whether the mitochondrial STING-MAVS interaction results in activation of the phospho-kinases promoting innate immune response, we performed confocal IF in post-cisplatin SCLC patient derived PBMCs to assess the subcellular of *p*-IRF3. As shown in Figures S3C and S3D, DNA-PKi induced a significant increase in *p*-IRF3 MFI ($p < 0.05$) and significantly promoted *p*-IRF3 translocation to the nuclear compartment ($p < 0.005$), thus confirming the functional interaction between STING and MAVS. Overall, these data suggest that DNA-PKi induces STING translocation to the mitochondria in post-cisplatin SCLC patients derived PBMCs, where it co-adapts with activated MAVS fibrils to strengthen the innate immune antitumor response. Additionally, DNA-PKi after chemo-immunotherapy-induced DNA stress further enhances and amplifies this mechanism by selectively activating MAVS fibrils formation. To strengthen the key contribution of MAVS in triggering STING activation upon DNA-PK inhibition, we performed silencing of MAVS in SCLC patients PBMCs collected post-cisplatin. We found that the efficacy of DNA-PKi and ENPP1i in activating STING downstream pathway was reduced in absence of MAVS even if the expression of total STING was not impaired (Figure S3E). In Figure S3F, we performed silencing of cGAS and STING in SCLC patient derived PBMCs to further confirm the non-canonical STING activation upon DNA-PKi treatment. We found that sicGAS specifically inhibited both *p*-IRF3 and STING in ENPP1i treated PBMCs, whereas DNA-PKi upregulated *p*-IRF3 and STING despite the silencing of cGAS. Furthermore, suppression of STING led to a reduction in the activation of this pathway in both DNA-PKi and ENPP1i-treated samples. Overall, these results confirm that DNA-PKi selectively induce MAVS activation and interaction with mitochondrial STING to activate and maintain the STING downstream pathway in immune cells independently from cGAS.

Based on these data, we studied the synergistic effect of the sequence of cisplatin followed by DNA-PKi in inducing an antitumor immune response in SCLC patients-derived PBMCs. Transcriptomic data showed that sequential treatment (cisplatin → DNA-PKi) significantly enriched viral infection-related signatures in patient-derived PBMCs (Figure S3G). We then compared the DEGs of sequential treatment compared to cisplatin alone. Interestingly, we found that sequential treatment prompts an enrichment in the IFN-induced antiviral response pathways as well as cytotoxic immune cell pathways ($CD8^+$ T cell pathway and NK cell-mediated cytotoxicity) in comparison to cisplatin in PBMCs (Figures 3D and S3H; Table S6), highlighting the efficacy of the sequential combination of cisplatin and DNA-PKi in sustaining an antitumor immune response. Overall, these results indicated that the non-canonical STING interaction with active MAVS fibrils induced by DNA-PKi after cisplatin efficiently activate anti-tumor immune response in SCLC patients PBMCs (Figure 3E).

DNA-PK inhibition effect on the interaction between MAVS and STING in PBMC-derived immune cells and SCLC cells

Next, we investigated the effect of DNA-PK inhibition in SCLC cells, alone or in coculture with PBMCs derived from SCLC patient's post-cisplatin. We first performed short-term treatments (6 h and 24 h) to verify the efficacy of DNA-PKi and ENPP1i in activating phosphorylation of kinases in the STING downstream pathway in SCLC cells by western blot (Figure S4A) and IF (Figures S4B and S4C). At 6 h, the two drugs show similar effects on activation of STING, MAVS, and downstream *p*-IRF3, while at 24 h ENPP1i is more effective in maintaining STING pathway downstream activation (with increased *p*-TBK1 and *p*-IRF3).

Instead, as shown in Figures 4A and 4B, when we conducted long-term treatments (72 h), we demonstrated the ability of DNA-PKi to maintain a prolonged immune response, as potentially needed in a clinical setting of maintenance therapy. Specifically, we showed that DNA-PKi treatment after 72 h in SCLC cell cultures upregulate MAVS lower band without activating the fibrils formation (upper band) (Figure 4A). In addition, it is not sufficient to impact STING expression. This finding was also confirmed by IP assay, which showed no MAVS/STING complex formation. Instead, DNA-PKi treatment after 72 h significantly increased *p*-IRF3 MFI compared to CTR and to ENPP1i (Figure 4B). However, *p*-IRF3 localized mainly in the mitochondrial compartment after treatment with DNA-PKi for 72 h. Based on these results, we hypothesized that DNA-PKi treatment alone was not sufficient to activate the non-canonical STING-MAVS activation in *in vitro* tumor cell lines. Therefore, we performed transcriptomic analysis to deeply understand these mechanisms in the context of SCLC cells. Gene set enrichment analysis (GSEA) showed a

Figure 3. Mechanism of non-canonical STING activation and mitochondrial localization induced by DNA-PK inhibition in SCLC patients-derived PBMCs

(A) Representative immunofluorescence images showing the MAVS (red) and STING (green) co-localization and ER-Tracker (blue) in immune cells treated with DNA-PKi and/or ENPP1i for 72 h (scale bar: 10 μm, Magnification 63×).

(B) Mean fluorescence intensity and merged area of confocal images determined by ImageJ software. The data are expressed as the means ± SD of 3 independent experiments.

$^{****}p < 0.0005$, $^{***}p < 0.005$, $^{**}p < 0.05$ (compared with the control group).

(C) Immunoprecipitation assay of MAVS in PBMC-derived lymphocytes from naive or under treatment SCLC patients. β-actin and IgG were used to ensure equal loading and as negative controls. At least three independent experiments were performed. Quantitative analysis of gel bands by morphodensitometric analysis using ImageJ software. Data are expressed as relative protein levels of each band compared to the corresponding equal loading ±SD.

(D) GSEA of RNA-seq data for SCLC patients-derived PBMCs treated with cisplatin followed by DNA-PKi versus cisplatin alone. Bars in red indicate a positive NES with significant enrichment in the treated samples, bars in gray represent gene sets with a negative NES and a significant enrichment in the control. Bars in black indicate the % of genes enriched in samples among the gene set analyzed.

(E) DNA-PK inhibition leads to alternative STING activation and mitochondrial recruitment to complex with MAVS and mediate immune cell activity. Image was created with the BioRender.com tool. See also Figure S3 and Table S6.

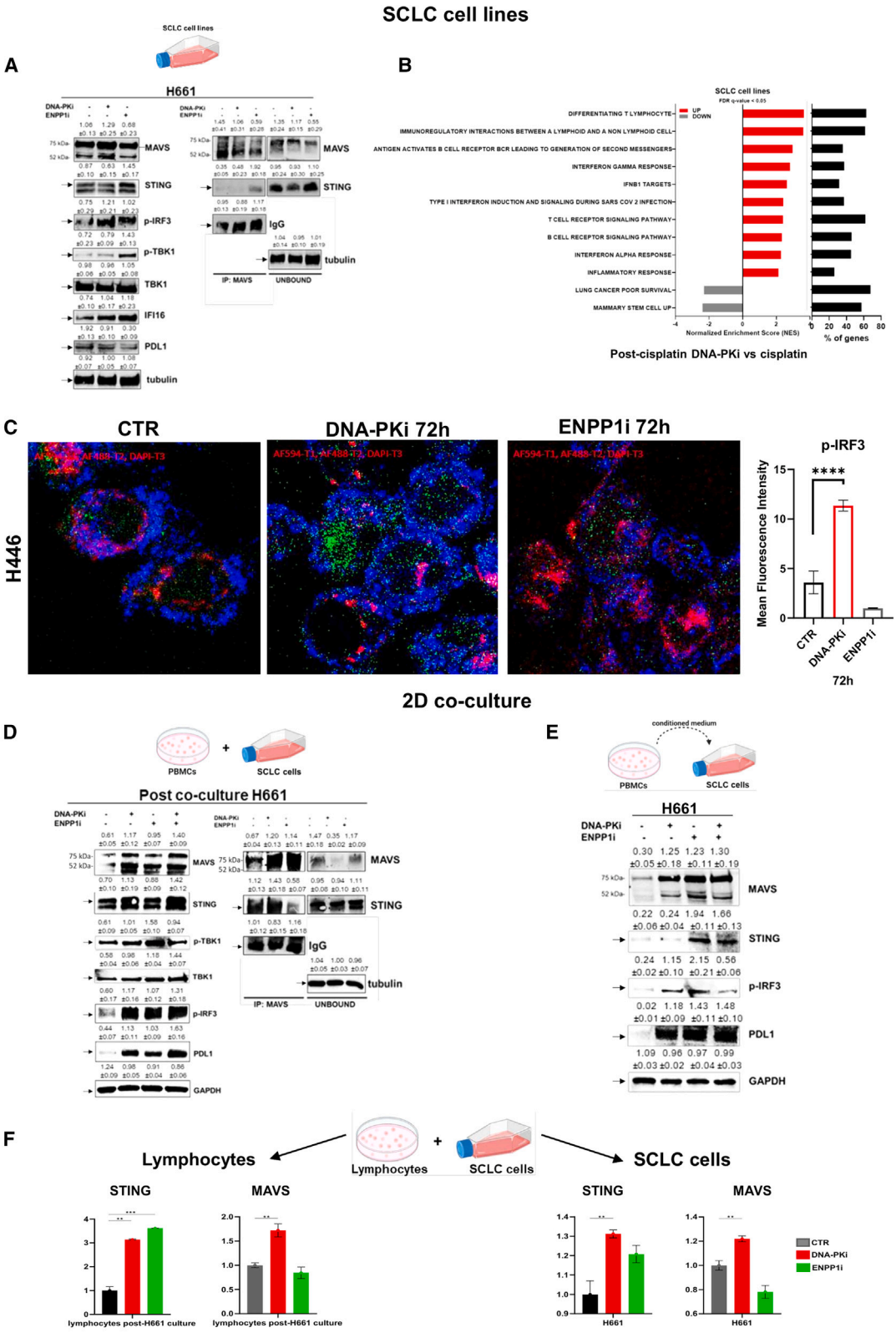

(legend on next page)

significant enrichment of the DNA repair and viral infection gene sets in SCLC cell lines treated with DNA-PKi, somewhat reproducing the cisplatin treatment effect (Figure S4D). Moreover, transcriptomic data showed that sequential treatment (cisplatin → DNA-PKi) vs. CTR significantly enriched IFN pathways and viral infection-induced IFN responses in SCLC cell lines. We also found a significant enrichment of apoptosis gene sets and a downregulation of metastasis and stem cells gene sets, thus suggesting an antitumor efficacy of the sequential treatment (Figure S4E). While, when we compared SCLC cell lines treated with the sequence vs. cisplatin alone, we found that sequential treatment induces higher upregulation of antitumor immune related pathways, specifically the T cell receptor and B cell receptor pathways, IFN-related pathways as well as the reduction of stem cells features, and the gene sets associated with lung cancer poor survival (Figures 4B and S4F; Table S7). These data indicated that DNA-PKi efficacy was most evident after a pre-existing chemotherapy damaged DNA in SCLC cells.

To assess whether facing immune cells could impact MAVS/STING activation in cancer cells, we established a 2D coculture of H661 (Figure 4C) and DMS79 (Figure S4G) SCLC cells with PBMCs derived from SCLC patient's post-cisplatin treatment. We found that physical contact between tumor cells and lymphoid cells strongly activates the non-canonical MAVS/STING pathway and induces physical complex assembly in tumor cells. Furthermore, we noted an upregulation of PD-L1 expression in the DNA-PKi-treated SCLC cells in coculture compared to SCLC alone, suggesting a potential benefit of combining DNA-PKi with immunotherapy after cisplatin treatment.

To verify whether these effects depend on physical contact or secretion of chemokine or other signaling molecules, we cultured SCLC cells with PBMC-conditioned medium for 48 h and then added DNA-PKi and/or ENPP1i for additional 72 h. In these conditions we found MAVS upregulation while we did not observe any significant differences in STING expression (Figure 4D), confirming that the non-canonical MAVS/STING activation requires the physical interactions between cancer cells and immune cells.

Next, we mechanically separated SCLC cells from lymphocytes or monocytes after coculture and analyzed them individually to clarify whether the non-canonical STING/MAVS pathway could be predominantly activated in immune cells subtypes or in cancer cells after coculture (Figures 4E and S4H). We selected different SCLC cell lines (DMS79, H446, and H661) and found an increase in STING/MAVS in DMS79 and H661 cells after treatment with DNA-PKi, but not in H446 cells. These results may be related to the intrinsic features of the cell line and should be the focus of future studies. For instance, different molecular features have been implicated in modulating sensitivity to DDR inhibitors in SCLC cells.[31] These results also confirmed the strong upregulation of both STING and MAVS in PBMC-derived lymphocytes and monocytes, independent of the cell line used in the coculture. The effect of the treatment on the mRNA expression levels of *STING*, *MAVS*, and *IFI16* in monocytes cultured alone is shown in Figure S4I. Together, these results provide the evidence that interaction between immune and cancer cells is needed for innate immune pathway activation and suggest that co-culture models represent a useful tool to investigate DNA/RNA sensors activation in the context of cancer-immune cells crosstalk.

Effect of DNA-PK inhibition on macrophage polarization and NK cell-mediated cytotoxicity

Since immune NK-mediated antibody-dependent cell-mediated cytotoxicity is a mechanism of response to immunotherapy in tumors with high PD-L1 expression[32] and can occur along with STING activation,[33] and considering the GSEA results that indicated an increased NK-cell mediated cytotoxicity after sequential treatment of cisplatin and DNA-PKi in SCLC patients-derived PBMCs, we investigated the antibody-dependent cell-mediated cytotoxicity ability of patient-derived immune cells against SCLC cell lines cocultured with DNA-PKi or ENPP1i. We performed LDH cytotoxicity assay by using an anti-CD16 NK cell-neutralizing antibody as a negative control to assess whether the DNA-PKi-induced cytotoxicity was mediated by NK cells subpopulation. Furthermore, to better observe NK cell activity or blockade, we selected DMS79 and H1882 PD-L1-high cell lines. Neutralization of the NK cells subpopulation strongly reduced the cytotoxic effect on both PD-L1 high SCLC cell lines (Figure 5A), indicating that DNA-PKi-induced cytotoxicity in this model is mainly mediated by NK cells. Furthermore, on the basis of the differential

Figure 4. Effect of DNA-PK inhibition on MAVS and STING interactions in SCLC cells culture and co-culture models

(A) Western blot analysis of total protein lysate (left) or immunoprecipitation with the MAVS antibody (right) in H661 culture SCLC cells untreated or treated with DNA-PKi or ENPP1i at a concentration of 2 μM for 72 h.

(B) GSEA of RNA-seq data for SCLC cell lines treated with cisplatin followed by DNA-PKi versus cisplatin alone. Bars in red indicate a positive NES with significant enrichment in the treated samples, bars in gray represent gene sets with a negative NES and a significant enrichment in the control. Bars in black indicate the % of genes enriched in samples among the gene set analyzed.

(C) Representative immunofluorescence images and MFI quantification showing *p*-IRF3 (green), MitoTracker (red) and DAPI (blue) in SCLC cells treated with DNA-PKi or ENPP1i (scale bar: 10 μm, Magnification 63×).

(D) Western blot analysis of total protein lysates (left) or immunoprecipitates (right) from H661 SCLC cells cocultured with PBMC-derived lymphocyte 48 h before adding treatment with 2 μM DNA-PKi or/and ENPP1i for 72 h.

(E) Protein expression analysis by western blot analysis of STING/MAVS pathway activation in H661 SCLC cells cultured in medium conditioned by patient-derived PBMCs with and/or without DNA-PKi or ENPP-1 (2 μM) for 72 h. Tubulin and GAPDH were used to ensure equal loading. At least three independent experiments were performed. Quantitative analysis of gel bands by morphodensitometric analysis using ImageJ software. Data are expressed as relative protein levels of each band compared to the corresponding equal loading ±SD.

(F) RT-PCR analysis of SCLC cells and SCLC patients derived lymphocytes after coculture for 48 h and treated with 2 μM DNA-PKi or/and 2 μM ENPP1i for 72 h. Normalized expression data are presented as the means ± S.E.M. derived from $n = 3$ technical calculations via the comparative method $2^{-\hat{}}(\Delta\Delta Ct)$ (reference gene 18S). One-tailed unpaired Student's t test with CI = 95%, ****$p < 0.0005$, ***$p < 0.005$, **$p < 0.05$. See also Figure S4 and Table S7.

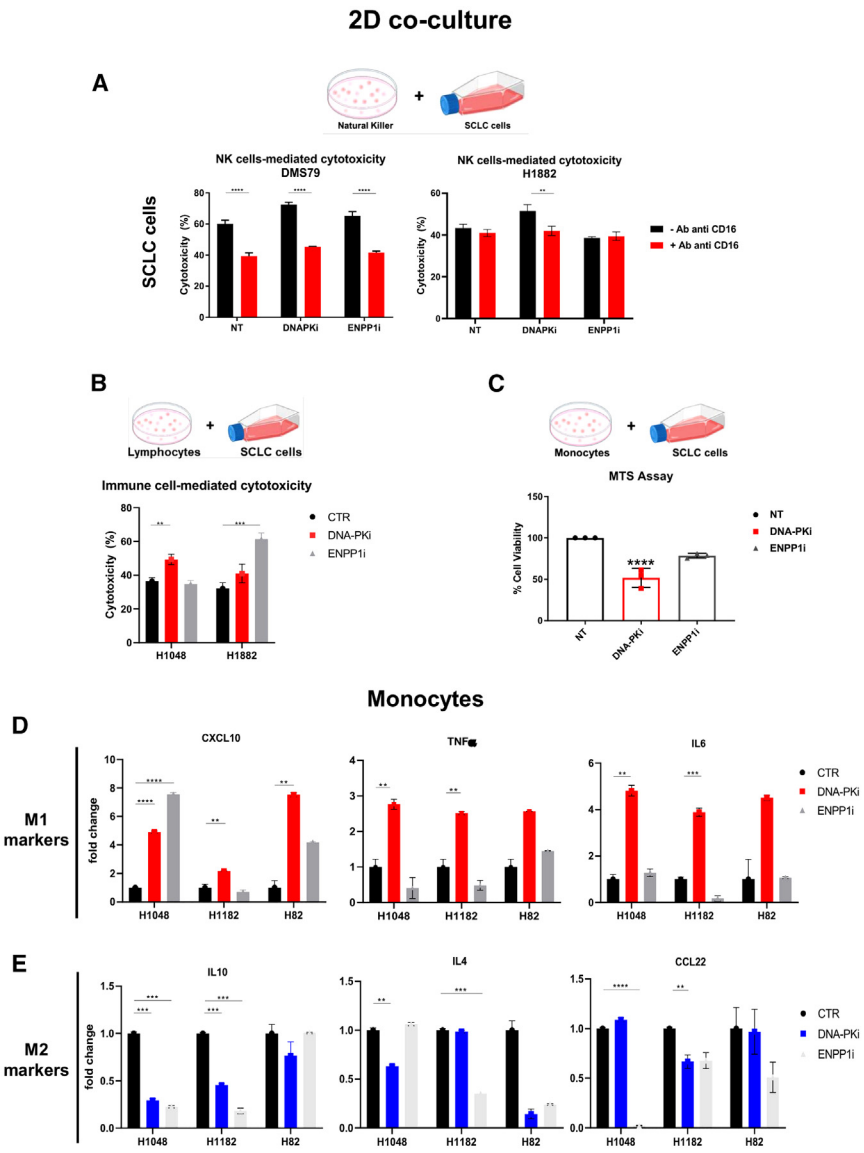

Figure 5. Effect of DNA-PK inhibition on SCLC patient-derived macrophage polarization and NK cell-mediated cytotoxicity

(A) LDH cytotoxicity assay of H1882 and H1048 SCLC cells after coculture with peripheral blood-derived lymphocytes for 5 days (ratio 1:4) and treated with DNA-PKi or ENPP1i for 72 h.

(B) LDH cytotoxicity assay on DMS79 and H1882 cancer cell lines cocultured with immune cells pretreated or not with anti-CD16 neutralizing antibody and then treated with DNA-PKi or ENPP1i for 72 h.

(C) MTS proliferation assay of SCLC cell lines (H1048, H1882, and H446) after 5 days of coculture with monocytes (ratio of 1:4) treated with 2 μM DNA-PKi or ENPP1i for 72 h.

(D and E) The mRNA expression of M1 and M2 markers was studied by RT-PCR and normalized to 18S expression. The results are expressed as the means ± 1 S.E.M. ($n = 3$). One-tailed unpaired Student's t test with CI = 95%, $^{****}p < 0.0005$, $^{***}p < 0.005$, $^{**}p < 0.05$.

effect of ENPP1i on whole PBMCs or NK cells only, we speculate that ENPP1i-induced immune cell-mediated cytotoxicity may be due to engagement of other immune subpopulations. As reported in Figure 5B, SCLC patients-isolated lymphocytes cytotoxicity was significantly increased after DNA-PKi treatment in H1048 cells ($p < 0.05$). In contrast, a significant cytotoxic effect ($p < 0.005$) was observed in H1882 cells treated with ENPP1i (Figure 5D). It is possible that other mechanisms could be responsible for the cytotoxic effect observed in H1882 cells treated with ENPP1i and deserve further investigations.

The M1/M2 macrophage paradigm plays a critical role in the pathogenesis of cancer, with M2-polarized macrophages having pro-tumoral features.[34] Therefore, we established a model for studying the effect of DNA-PKi on macrophage polarization, starting from under treatment SCLC patient-derived monocytes. As described previously, we mechanically isolated monocytes from PBMCs by adhesion to a well plate for 1 h. Next, monocytes and H1048, H1882, or H82 cancer cells were cocultured for 48 h before DNA-PKi or ENPP1i exposure (2 μM) for additional 72 h. After incubation, the impact of treatment on monocyte polarization to M1 (pro-inflammatory and anti-tumoral) or M2 (anti-inflammatory and pro-tumoral) was studied, and cancer cell proliferation was assessed using the MTS assay. DNA-PKi decreased cancer cells viability when cocultured with monocytes. Blockade of ENPP1 in monocytes slightly reduced the viability of H1048, H82, and H1882 cells (81.12%, 75.55%, and 78.89%, respectively) (Figure 5C). We then collected monocytes after coculture with cancer cells and we performed analysis of M1/M2 polarization. M1 polarization was assessed by measuring the mRNA expression of the classical M1 markers *TNFA*, *IL-6*, and *CXCL10*, which are pro-inflammatory cytokines (Figure 5D). DNA-PKi increased the expression of pro-inflammatory markers. *TNFA* and *IL-6* were not overexpressed in ENPP1i-treated monocytes, whereas *CXCL10* expression was significantly increased in ENPP1i-treated monocytes. This finding is consistent with CXCL10 being a downstream target of the canonical cGAS-STING pathway and with the STING agonists being potent inducers of type I IFN-regulated chemokines (CXCL9 and CXCL10). Polarization of macrophages into alternatively activated macrophages, also known as M2 cells, is induced *in vivo* by IL-4 and IL-13. We also measured the mRNA expression of M2 markers (*IL-10*, *IL4*, and *CCL22*) in PBMC-derived monocytes cocultured with SCLC cell lines; however, in our conditions, we did not observe any significant increase in the expression of these genes, with the exception of *CCL22* increase in H1048 cells (Figure 5E). Overall, we suggest that DNA-PKi induces

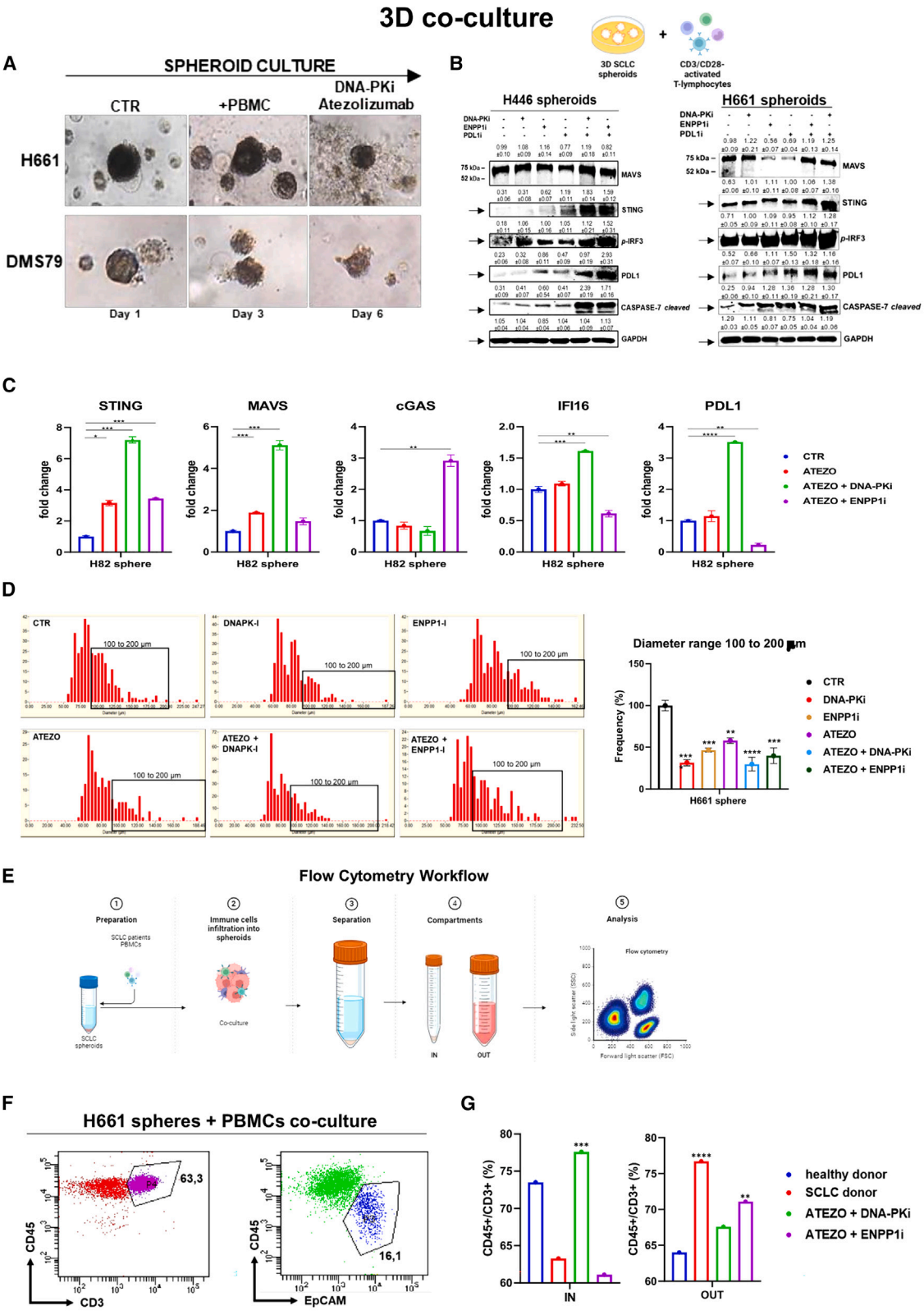

(legend on next page)

anti-tumoral phenotypes in multiple SCLC patients-derived PBMCs thus promoting features of immune responsiveness and immune-cells mediated cytotoxicity.

Effect of DNA-PK inhibition on 3D coculture spheroids and PBMC-derived immune cells

We have previously shown that co-culturing 3D spheroids from cell lines with patient-derived PBMCs is a valid surrogate for autologous models to functionally predict therapy-induced immune activation *in vitro*.[22] To test the direct antitumor efficacy and potential antitumor immunity of the strategy using DNA-PKi plus immunotherapy (atezolizumab 10 μg/mL), we used 3D cocultures of SCLC cells grown as spheroids and PBMC-derived suspension lymphocytes. We estimated the ability of lymphocytes to migrate toward SCLC spheroids using this *in vitro* system. Spheroids from SCLC cell lines (H661, DMS79, H82, and H446) were obtained *in vitro* and SCLC PBMC-derived lymphocytes were added for 3 days. Cocultures were monitored and imaged, revealing the migration of immune cells in the plates toward the tumor spheroids. On day 3 of coculture, we added treatments for an additional 72 h and imaged the cells before analysis (Figure 6A). Subsequently, we analyzed the tumor spheroids for changes in gene and protein expression. Western blot analysis showed elevated expression levels of MAVS fibrillar form (upper band), STING and activation of the downstream signaling pathway (*p*-IRF3) in cells treated with DNA-PKi plus atezolizumab. Treatment with ENPP1i and atezolizumab as single agents also activated the STING pathway, but with lower efficacy than the combination. Moreover, atezolizumab plus DNA-PKi increased levels of cleaved caspase-7 in SCLC cells grown as spheroids in coculture with immune cells (Figures 6B and S5A). In addition, a significant increase in *STING* ($p < 0.005$), *MAVS* ($p < 0.005$), *IFI16* ($p < 0.005$), and *PD-L1* ($p < 0.0005$) gene expression levels was detected by RT-PCR in H82 cells grown as spheroids in 3D coculture and treated with the combination of atezolizumab plus DNA-PKi. Interestingly, *cGAS* levels did not increase after DNA-PK inhibition in combination with atezolizumab, confirming that DNA-PK inhibition induces STING upregulation independently of cGAS in SCLC cells (Figure 6C). This effect, together with immune cell-mediated cytotoxicity on tumor cells, results in the destruction of SCLC-derived spheroids *in vitro*. To quantify the antitumor effect, we analyzed the changes in tumorsphere size (expressed in the diameter range) induced by the treatments. Figure 6D shows a reduction in the diameter range (100–200 μm) of tumor spheroids treated with DNA-PKi alone (frequency range FR 31.5%) and in combination with atezolizumab (FR 28.8%) compared to those treated with DNA-PKi alone (FR 46.7%), atezolizumab alone (FR 58.1%) or ENPP1i combined with atezolizumab (FR 29.8%). These results indicate that combination therapy with DNA-PKi and atezolizumab directly activated immune cells to disrupt the 3D spheroid structure. To confirm that the reduction in sphere diameter was due to enhanced immune cell activity and tumor sphere infiltration, we performed FACS analysis on 3D coculture and measured the percentages of infiltrating (IN) and noninfiltrating (OUT) immune cells as previously described[35] (Figure 6E). By comparing the cellular proportions IN and OUT of the untreated spheroids, we observed a greater proportion of $CD45^+CD3^+$ lymphocytes in the spheroid structure (IN compartment) in PBMCs from healthy donors (73.8%) than in PBMCs from SCLC patients (63.2%), suggesting a slight reduction in immune cell infiltration ability in SCLC patients compared to that in healthy donor-derived immune cells (Figures 6F and S5B). This result suggests that the immune response could be intrinsically altered in patients with SCLC, thus requiring further studies and supporting the need for strategies for immune activation in these patients.[36] We then tested the possibility of modulating the immune response in this system by adding atezolizumab plus DNA-PKi or ENPP1i to the cocultures. Combined treatment with atezolizumab plus DNA-PKi strongly increased spheroid infiltration by SCLC patient-derived lymphocytes, which accounted for 75.7% of the total immune cells infiltrated per spheroid compared to 64.3% of the infiltrating immune cells in the ENPP1i plus atezolizumab spheroids (Figure 6G). All these data on the effects of DNA-PKi and atezolizumab on SCLC models could be further extended in the future with *in vivo* studies to measure direct changes in intratumor infiltration.

Effect of DNA-PK inhibition in ex-vivo SCLC cells derived from patient's MPE

Here, we aimed to establish an *ex vivo* model to validate the role of DNA-PKi in activating STING/MAVS innate immune pathway

Figure 6. Effect of DNA-PK inhibition on 3D cocultured SCLC spheroids and PBMC-derived immune cells

(A) Representative images of SCLC cell lines grown as spheroids and monitored over six days. On day 3, the PBMC-derived lymphocyte suspensions were added to the spheroids. After 48 h, DNA-PKi or ENPP1i (4 μM) plus atezolizumab (10 μg/mL) was added for an additional 72 h. Bright field images were taken daily. Magnification: 20× objective.

(B) Western blot analysis of STING/MAVS expression and downstream signaling pathway components in the total protein lysates of H446 and H661 spheroids cocultured for 5 days with SCLC patient-derived PBMCs and treated for 72 h with DNA-PKi or ENPP1i (4 μM) plus atezolizumab (10 μg/mL). GAPDH was used to ensure equal loading. At least three independent experiments were performed. Quantitative analysis of gel bands by morphodensitometric analysis using ImageJ software. Data are expressed as relative protein levels of each band compared to the corresponding equal loading ±SD.

(C) RT-PCR of H82 spheroids cocultured with PBMC-derived immune cells in complete media for 48 h and then treated with atezolizumab (10 μg/mL) plus DNA-PKi or ENPP1i (4 μM) for 72 h. Normalized expression data are presented as the means ± S.E.M. derived from $n = 3$ technical calculations via the comparative method $2^{-}(\Delta\Delta Ct)$ (reference gene 18S). One-tailed unpaired Student's t test with CI = 95%, $^{****}p < 0.0005$, $^{***}p < 0.005$, $^{**}p < 0.05$.

(D) The change in spheroid diameter following treatment was quantified using GelCount software. The frequency ranges (%) data are presented as the means ± SD ($n = 4$).

(E) Graphical summary of experimental workflow for flow cytometry analysis of infiltrating lymphocytes in SCLC spheroids. Image was created with the BioRender.com tool.

(F and G) Flow cytometry analyses of immune cell ($CD3^+$ among live single cell lymphocytes) percentages in the IN and OUT compartments, in the presence or absence of atezolizumab plus DNA-PKi or ENPP1i at 72 h. See also Figure S5.

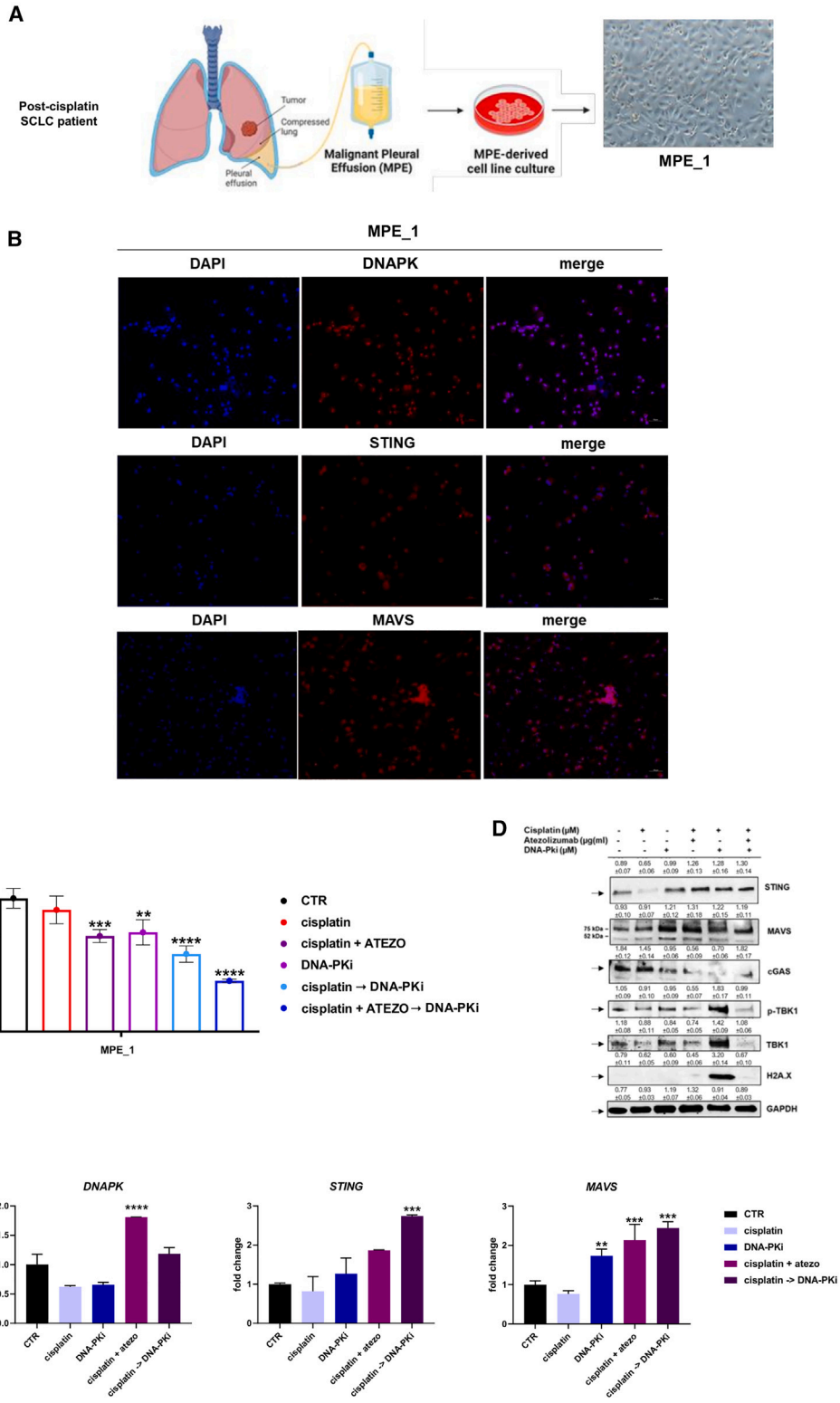

(legend on next page)

in the context of maintenance therapy. In this regard, the lack of adequate tissue samples from diagnostic biopsies of SCLC patients leads to a general lack of opportunities to investigate SCLC biology in *ex vivo* models. Therefore, we established MPE-derived cell line from SCLC patient undergoing maintenance treatment with atezolizumab (MPE_1). The morphology of the established cell line was predominantly oval and round, with some cells having a fibroblast-like shape (Figure 7A). We showed activation of DNA-PK and immune pathway in MPE_1 culture by assessing the expression of DNA-PK and DNA/RNA sensors STING and MAVS by immunofluorescence (Figure 7B).

Then we tested the effect of cisplatin (0.5 μM) alone and combined with atezolizumab (10 μg/mL) and/or with DNA-PKi (2 μM) for 72 h with the aim of proving the efficacy of sequential treatment with DNA-PKi after cisplatin treatment. We found that sequential treatment with cisplatin + atezolizumab → DNA-PKi ($p < 0.0005$) induced the most significant reduction of cell viability (%) (Figure 7C). We then performed western blot to assess whether the addition of DNA-PKi post-cisplatin may influence DNA/RNA sensor innate immunity activation to confirm the results obtained in *in vitro* and 2D/3D co-culture models previously presented. We found that the expression of STING and MAVS was increased by the addition of DNA-PKi after cisplatin or chemo-immunotherapy. Interestingly, the sequential treatment of cisplatin → DNA-PKi strongly increased the innate immune response through TBK1 protein phosphorylation and overexpression as compared to untreated control. In addition, the activation of STING downstream pathway is independent from cGAS expression, thus indicating the occurrence of non-canonical MAVS/STING activation upon DNA-PKi. This effect occurred along with a significant increase of DNA damage marker (H2A.X) in cisplatin → DNA-PKi MPE_1 cells (Figure 7D). We also confirmed western blot results by RT-PCR which showed a significant increase of *DNAPK* ($p < 0.0005$) and *MAVS* ($p < 0.0005$) after chemo-immunotherapy treatment. Moreover, the addition of DNA-PKi post-cisplatin strongly increased both *STING* ($p < 0.0005$) and *MAVS* ($p < 0.0005$) thus confirming that the addition of DNA-PKi post-chemotherapy plays a key role in sustaining multiple DNA/RNA sensors innate immune pathways (Figure 7E). In particular, since the MPE_1 cells were derived after chemotherapy treatment in SCLC patient and may potentially represent a sub-population of resistant cells, the increase in DNA-PK after chemo-immunotherapy suggested that its targeting can prevent therapeutic resistance.

DISCUSSION

SCLC is biologically characterized by high intrinsic DNA damage due to the universal loss of *TP53* and the retinoblastoma gene (*RB1*).[7] Our group and others have previously demonstrated that the combination of DDRis (such as PARPi, Chk1i, and WEEi) and immunotherapy plays a positive role in the immune response via the STING-dependent activation of PD-L1 and T lymphocytes[37]. We also previously demonstrated that activation of the cGAS-STING signaling pathway in PBMCs from SCLC patients may be a potential predictive biomarker for response to immunotherapy, and high expression levels of STING are correlated with a better response to treatment.[22] Thus, STING activation is a confirmed mechanism for enhancing SCLC immune responsiveness, but unfortunately, it is not easy to translate in a clinical setting, since STING agonists have low clinical applicability, and can be used only for local intratumoral administration.[38]

In the present study, we investigated the effect on induction of antitumor immune response of sequential treatment with cisplatin and DNA-PKi in SCLC cells, patients-derived immune cells and co-coculture systems and *ex vivo* models of SCLC cells isolated from MPE. By performing GSEA on RNA-seq data obtained from SCLC cell lines and SCLC patient-derived PBMCs treated with cisplatin, we demonstrated that chemotherapy-induced DNA damage and inhibition of the DDR pathway activate innate immune-related IFN signaling pathways. Interestingly, we showed that the addition of sequential treatment with DNA-PKi after cisplatin led to maintenance of the innate immune response, IFN-related pathways as well as $CD8^+$ T cell and NK-cell activation pathways, thus confirming the efficacy of DNA-PKi after chemo-immunotherapy. In this regard, the cytotoxic effect of cisplatin activates DDR pathway and can also lead to the release of cytosolic DNA fragments that activate STING, thereby enhancing the recruitment and activation of immune cells through IRF3 nuclear translocation.[39,40] Given the immunogenic potential of cisplatin-induced DNA damage, there is a compelling rationale for utilizing DDR inhibitors as maintenance therapy following chemotherapy.[41,42] Through a comprehensive *in vitro* characterization using functional assays, we proved that DNA-PKi sustains a widespread antitumor immune response through noncanonical STING-MAVS complex activation in both SCLC cell lines and immune cells, somewhat reproducing the antiviral response.[19] In detail, we show that DNA-PKi enhances STING activity by facilitating its translocation to mitochondria, where it forms complexes with MAVS further amplifying immune

Figure 7. Effect of DNA-PKi on MPE-derived cell line isolated from SCLC patient

(A) Schematic representation of cell line isolation from MPE of SCLC patient (Magnification 20×).

(B) Representative immunofluorescence image showing the DNA-PK, STING and MAVS (red) in SCLC MPE-derived cells isolated from resistant SCLC patient (scale bar 50 μm).

(C) Cell Viability assay on pleural fluid-isolated SCLC patient cancer cells. Cells were plated in 6 well and treated with cisplatin (0.5 μM) either alone or combined with anti-PD-L1 atezolizumab (10 μg/mL) or DNA-PKi (2 μM) for 72 h. Sequential treatment of cisplatin alone or combined with atezolizumab for 24 h followed by addition of DNA-PKi for further 48 h was performed.

(D) Western blot analysis of DNA damage and STING/MAVS expression and downstream signaling pathway components in the total protein lysates of SCLC MPE-derived cells treated for 72 h with cisplatin (0.5 μM), DNA-PKi (2 μM) and/or atezolizumab (10 μg/mL). GAPDH was used to ensure equal loading. At least three independent experiments were performed. Quantitative analysis of gel bands by morphodensitometric analysis using ImageJ software. Data are expressed as relative protein levels of each band compared to the corresponding equal loading ±SD.

(E) RT-PCR of SCLC MPE-derived cells treated with cisplatin (0.5 μM), DNA-PKi (2 μM) and/or atezolizumab (10 μg/mL). ****$p < 0.0005$, ***$p < 0.005$, **$p < 0.05$.

signaling. This mechanism could explain how DNA-PKi can sustain an active immune response after the induction of chemotherapy, promoting antitumor immunity. In addition, this STING-MAVS complex is more likely to occur when DNA-PKi treatment is performed in PBMCs derived from SCLC patients under chemo-immunotherapy treatment compared to naive patients, suggesting that this phenomenon may deserve further investigation as potential biomarker in patients.

Various studies have reported that high-NE SCLC lines grow as non-adherent floating aggregates that do not express STING, whereas low-NE SCLC cell lines grow as loosely adherent cells with STING derepression.[43–45] We showed that the highest basal levels of STING were detected in H661 (adherent) cells compared to those in SCLC cell lines growing in suspension (H82, H2141, H524, and H209) or mixed (H446). Although the STING pathway is less transcriptionally active in the NE form, in our coculture systems, interaction with immune cells may impact basal STING expression levels. This phenomenon is accompanied by positive changes in immune cell metabolism, macrophage polarization, and NK cell activation.

Several studies indicate that combining DDR inhibitors with immune checkpoint inhibitors may synergistically improve therapeutic outcomes in relapsed SCLC by converting ''cold'' tumors into ''hot'' tumors through enhanced immune cell infiltration and activation.[42,46] Thus, to model the clinical efficacy of our results, we demonstrated that the combination of DNA-PKi and anti-PD-L1 drugs induced immune-mediated antitumor effects in *in vitro* 3D cocultures of SCLC cells and PBMCs, as shown by the increased ability of lymphocytes to infiltrate tumor spheroids. These results are consistent with those of other studies using tumor spheroids as tools to investigate tumor-lymphocyte interactions.[35] The advantage of this 3D cocultures system derives from its simple, cheap, and fast setup and great adaptability to various culture conditions, thus enabling the analysis of dynamic and differential inter-patient responses in a controlled environment.

Specifically, we found that chemo-immunotherapy and DNA-PKi stress stimuli increased the intracellular protein levels of STING and full-length MAVS, which is the MAVS isotype capable of forming large prion-like fibril complexes on the mitochondrial membrane.[28] MAVS is active only when it is bound to the mitochondria; its cleavage and detachment from the mitochondria significantly reduces its ability to activate the IFN-I signaling pathway.[29]

Here, we also described a model of the interplay of innate immune pathways in SCLC induced by cytosolic nucleic acid fragments released under treatment pressure. Independently of the canonical activation of the STING pathway prompted by DNA fragmentation through cGAS, DNA-PKi selectively guides STING to translocate to the mitochondria, where it assembles into MAVS fibrils and induces potentiated antitumor immune signals. In all experimental models, we demonstrated the difference in canonical versus noncanonical STING activation using ENPP1i treatment (which instead drives cGAS activation) as a control for the canonical pathway. The formation of the STING-MAVS complex further potentiates the activation of downstream inflammatory and T cell-recruiting signals and potentially increasing immune-responsiveness. Also, while harnessing this active antitumor immune response, the strategy of combination of anti-PD-L1 with cisplatin followed by DNA-PKi induces direct cytotoxic effects on tumor cells. In fact, he addition of DNA-PKi serves to further inhibit DNA repair mechanisms that would potentially resolve cisplatin-induced damage. By blocking DNA-PK, these inhibitors prevent effective repair of the DNA cross-links formed by cisplatin, thereby sustaining tumor damage and the consequent activation of immune pathways initiated by the DDR.

Taken together, our findings provide a biological rationale for using DNA-PKi with immunotherapy in SCLC, based on the activation of the inflamed phenotype through a combined STING-MAVS response. Notably, we concluded that the use of DNA-PKi in clinical treatment may be most beneficial for preventing tumor progression in patients following chemo-immunotherapy, as we demonstrated in the established *ex vivo* model of SCLC isolated from MPE of SCLC patient after chemo-immunotherapy. Additionally, the combination of DNA-PKi and ENPP1i or other similar agents (chemo-, radio-therapy) that activate both the canonical and noncanonical pathways of STING may have greater application in other clinical setting of relapsed SCLC patients with the aim of resensitizing tumor to immunotherapy and in other tumor types. Considering that the combination of DNA-PKi, immunotherapy, and radiotherapy or in combination with cisplatin has already been tested in phase I clinical trials with a good safety profile,[47,48] our data support a rational for future studies in SCLC patients using PBMCs as biomarkers tool.

In conclusion, we identified an unexpected function of STING in the mitochondrial membrane: control of immune cell activation through a previously unrecognized STING-MAVS axis co-activated in SCLC and in immune cells upon DNA-PK inhibition. Collectively, our results support further investigations of the mechanisms, biomarkers, and efficacy of DNA-PKi and immunotherapy combinations in sustaining antitumor immune response after chemo-immunotherapy in SCLC patients.

Limitations of the study

The present study is subject to certain limitations inherent to the complex and heterogeneous nature of SCLC, particularly about the distinction between high-NE and low-NE subtypes that may have an impact on the applicability of the findings and suggest future explorations of these results in various subtypes of SCLC.

Regarding the models selected for the studies, the use of *in vitro* models, like 3D cocultures and patient-derived immune cells, while highly valuable for the direct link with clinical context, may not fully replicate the intricate tumor microenvironment found *in vivo*, potentially leading to an overestimation of immune-mediated antitumor effects. Therefore, future studies in *in vivo* models are needed to ascertain the effect over time of DNA-PKi in activating STING-MAVS-mediated innate immune pathway in SCLC immune and cancer cells.

In addition, we acknowledge the requirement for longitudinal studies to evaluate the long-term efficacy and safety of combining DNA-PKi with immunotherapy, particularly in light of the frequent rapid disease progression observed in SCLC patients. Finally, our analyses were based on a limited sample size, which could potentially impact the statistical power and broader applicability of our findings.

Collectively, these limitations underscore the necessity for further research to validate our results in terms of translational potential in clinical context.

RESOURCE AVAILABILITY

Lead contact

Further information and requests for resources and reagents should be directed to and will be handled by the lead contact, Carminia Maria Della Corte (carminiamaria.dellacorte@unicampania.it).

Materials availability

MPE-derived cell line generated in this study are available from the lead contact with a completed materials transfer agreement.

Data and code availability

- All RNA-seq data generated during this study have been deposited in the Sequence Read Archive (SRA) with BioProject ID: PRJNA1208015 and are publicly available as of the date of publication. This paper analyzes existing, publicly available tumor gene expression data, accessible via the European Genome-phenome Archive: EGAS00001000925.[26] Original western blot images have been deposited at Mendeley: https://doi.org/10.17632/x4xvsv6v39.1 and are publicly available as of the date of publication. Microscopy data reported in this paper will be shared by the lead contact upon request.
- This paper does not report original code.
- Any additional information required to respond to any question related to the data reported in this paper is available from the lead contact upon request.

ACKNOWLEDGMENTS

This study has been funded by MFAG AIRC (Project Number: 26237) (C.M.D.C), NIH/ NCI R01-CA207295 (L.A.B), NIH/ NCI U01- CA256780 (L.A.B), NIH/ NCI P50-CA070907 (L.A.B), and NIH/ NCI P30-CA016672 (L.A.B). We would like to acknowledge Novogene Corporation Inc. for RNA-seq analysis. We thank Dr. Ludovica D'Auria for assisting and for providing the Microscopy Facility at CEINGE-Biotecnologie Avanzate (Naples, Italy).

AUTHOR CONTRIBUTIONS

Conceptualization: C.M.D.C., C.D.R., and F.M.; data curation: C.D.R., F.M., L.A., C.T., K.R., Q.W., and J.W.; formal analysis: V.T., F.P., S.Z., M.C., A.G., and V.N.; funding acquisition C.M.D.C.; investigation: C.M.D.C., C.D.R., F.M., F.I., and V.D.R.; methodology: C.D.R., F.M., L.A., F.I., V.D.R., V.T., F.P., C.T., G.D.G., D.M.D., A.D.L., D.C., S.N., G.M., and A.S.; project administration: C.M.D.C., K.R., F.D.V., E.M., T.T., S.N., G.M., A.S., L.A.B., and F.C.; resources: F.M., F.I., V.D.R., V.T., F.P., S.Z., A.G., L.A.B., F.C., and C.M.D.C.; software: C.D.R., L.A., K.R., Q.W., J.W., and L.A.B.; supervision: C.M.D.C., F.C., and C.T.; validation: F.I., V.D.R., V.T., and F.P.; visualization: C.D.R., F.M., L.A., D.C., S.N., and G.M.; writing—original draft: C.D.R., F.M., L.A., D.C., S.N., and G.M.; writing—review and editing: C.M.D.C., F.C., L.A.B., F.I., V.D.R., V.T., F.P., K.R., F.D.V., E.M., T.T., and A.S.

DECLARATION OF INTERESTS

Dr. Morgillo F. Received honoraria or consultation fees for speaker, consultancy, or advisory roles: Roche, Servier, Incyte, ESMO, and MSD. Dr. Papaccio F.: Private research funding from Merck, travel support from Diatech Pharmacogenetics, and recipient of an ESMO Research Fellowship sponsored by Amgen from 2018 to 2020. Dr Ciardiello D.: travel support from Sanofi, BMS and Merck KgA. Dr. Martinelli E.: Receipt of honoraria or consultation fees for speaker, consultancy, or advisory roles: Amgen, Bayer, Eisai, Merck Serono, Pierre Fabre, Roche, Servier, Incyte, ESMO, MSD; Travel grant: AstraZeneca, Pierre Fabre. Dr. Troiani T. Receipt of honoraria or consultation fees for speaker, consultancy, or advisory roles: Merck, Amgen, Pierre Fabre, Servier, MSD, Bayer, and Novartis. Dr. Napolitano S. received travel grants from Amgen, Merck KGaA, Bristol Myers Squibb, and Novartis outside the submitted work. Dr Martini G. reported receiving honoraria from Servier and Incyte outside the submitted work. Dr. Servetto A: Speaker Honoraria from Eli Lilly, MSD, Janssen, Roche, Novartis, and Gilead; Travel support from Bristol-Myers Squibb and AstraZeneca; Board advisor: MSD. Dr. De Vita F. serves consulting/advisory role for Roche, Bayer, BMS, Servier, Lilly, Astellas, MSD, Merck, Astra Zeneca, Dajichi. Dr. Byers L. received honoraria from Clinical Cancer Care Options, research funding from AstraZeneca, Amgen and Jazz Pharmaceuticals and serves consulting/advisory roles for Merck Sharp & Dohme Corp., Arrowhead Pharmaceuticals, Chugai Pharmaceuticals Co., AstraZeneca Pharmaceuticals, Genentech Inc., AbbVie, BeiGene, Jazz Pharmaceuticals, Puma Biotechnology, Amgen, Daiichi Sankyo, Boehringer Ingelheim, and Novartis. Dr. Ciardiello F. Receipt of honoraria or consultation fees for speaker, consultancy, or advisory roles: Amgen, Merck KGaA, MSD, Pierre Fabre, Pfizer, Roche, Servier; Institutional financial interests, financial support for clinical trials or contracted research; Amgen, Merck KGaA, MSD, Pierre Fabre, Pfizer, Roche, Servier. Dr. Della Corte C.M. reported receiving personal fees from Roche, MSD, and AstraZeneca, and travel grants from Amgen outside the submitted work.

STAR★METHODS

Detailed methods are provided in the online version of this paper and include the following:

- KEY RESOURCES TABLE
- EXPERIMENTAL MODEL AND STUDY PARTICIPANT DETAILS
  - Study approval
  - Sample size estimation
  - How subjects/samples were allocated to experimental groups
  - General informations on partecipants
  - Cell lines
- METHOD DETAILS
  - Peripheral blood mononuclear cells (PBMCs) isolation
  - Reagents
  - RNA-sequencing analysis
  - Gene expression
  - RNA extraction and cDNA synthesis
  - Gene expression analysis by quantitative reverse transcription-polymerase chain reaction (qRT-PCR)
  - Western blot analysis
  - Immunoprecipitation
  - Immunofluorescence
  - Cell energy phenotype and glycolytic rate assay
  - RNA interference
  - MTS assay
  - Lactate dehydrogenase cytotoxicity assay
  - Spheroid formation and 3D coculture protocol
  - Flow cytometry
  - Establishment of cell line from Malignant Pleural Effusion of SCLC patient
- QUANTIFICATION AND STATISTICAL ANALYSIS

SUPPLEMENTAL INFORMATION

Supplemental information can be found online at https://doi.org/10.1016/j.isci.2025.111943.

Received: August 20, 2024
Revised: November 20, 2024
Accepted: January 29, 2025
Published: February 1, 2025

REFERENCES

1. Horn, L., Mansfield, A.S., Szczęsna, A., Havel, L., Krzakowski, M., Hochmair, M.J., Huemer, F., Losonczy, G., Johnson, M.L., Nishio, M., et al.

(2018). First-Line Atezolizumab plus Chemotherapy in Extensive-Stage Small-Cell Lung Cancer. N. Engl. J. Med. *379*, 2220–2229. https://doi.org/10.1056/NEJMoa1809064.

2. Liu, X., Xing, H., and Liu, B. (2022). Current status and future perspectives of immune checkpoint inhibitors in extensive-stage small cell lung cancer. Am. J. Cancer Res. *12*, 2447–2464.
3. Paz-Ares, L., Dvorkin, M., Chen, Y., Reinmuth, N., Hotta, K., Trukhin, D., Statsenko, G., Hochmair, M.J., Özgüroğlu, M., Ji, J.H., et al. (2019). Durvalumab plus platinum-etoposide versus platinum-etoposide in first-line treatment of extensive-stage small-cell lung cancer (CASPIAN): a randomised, controlled, open-label, phase 3 trial. Lancet *394*, 1929–1939. https://doi.org/10.1016/S0140-6736(19)32222-6.
4. Saltos, A., Shafique, M., and Chiappori, A. (2020). Update on the Biology, Management, and Treatment of Small Cell Lung Cancer (SCLC). Front. Oncol. *10*, 1074. https://doi.org/10.3389/fonc.2020.01074.
5. Gay, C.M., Stewart, C.A., Park, E.M., Diao, L., Groves, S.M., Heeke, S., Nabet, B.Y., Fujimoto, J., Solis, L.M., Lu, W., et al. (2021). Patterns of transcription factor programs and immune pathway activation define four major subtypes of SCLC with distinct therapeutic vulnerabilities. Cancer Cell *39*, 346–360. https://doi.org/10.1016/j.ccell.2020.12.014.
6. Sen, T., Rodriguez, B.L., Chen, L., Corte, C.M.D., Morikawa, N., Fujimoto, J., Cristea, S., Nguyen, T., Diao, L., Li, L., et al. (2019). Targeting DNA Damage Response Promotes Antitumor Immunity through STING-Mediated T-cell Activation in Small Cell Lung Cancer. Cancer Discov. *9*, 646–661. https://doi.org/10.1158/2159-8290.CD-18-1020.
7. Byers, L.A., Wang, J., Nilsson, M.B., Fujimoto, J., Saintigny, P., Yordy, J., Giri, U., Peyton, M., Fan, Y.H., Diao, L., et al. (2012). Proteomic profiling identifies dysregulated pathways in small cell lung cancer and novel therapeutic targets including PARP1. Cancer Discov. *2*, 798–811. https://doi.org/10.1158/2159-8290.CD-12-0112.
8. Cardnell, R.J., Feng, Y., Diao, L., Fan, Y.H., Masrorpour, F., Wang, J., Shen, Y., Mills, G.B., Minna, J.D., Heymach, J.V., and Byers, L.A. (2013). Proteomic markers of DNA repair and PI3K pathway activation predict response to the PARP inhibitor BMN 673 in small cell lung cancer. Clin. Cancer Res. *19*, 6322–6328. https://doi.org/10.1158/1078-0432.CCR-13-1975.
9. Sen, T., Gay, C.M., and Byers, L.A. (2018). Targeting DNA damage repair in small cell lung cancer and the biomarker landscape. Transl. Lung Cancer Res. *7*, 50–68. https://doi.org/10.21037/tlcr.2018.02.03.
10. Li, W., Lu, L., Lu, J., Wang, X., Yang, C., Jin, J., Wu, L., Hong, X., Li, F., Cao, D., et al. (2020). cGAS-STING-mediated DNA sensing maintains CD8. Sci. Transl. Med. *12*, eaay9013. https://doi.org/10.1126/scitranslmed.aay9013.
11. Liu, D., Lum, K.K., Treen, N., Núñez, C.T., Yang, J., Howard, T.R., Levine, M., and Cristea, I.M. (2023). IFI16 phase separation via multi-phosphorylation drives innate immune signaling. Nucleic Acids Res. *51*, 6819–6840. https://doi.org/10.1093/nar/gkad449.
12. Moresco, E.M.Y., Vine, D.L., and Beutler, B. (2011). Prion-like behavior of MAVS in RIG-I signaling. Cell Res. *21*, 1643–1645. https://doi.org/10.1038/cr.2011.155.
13. Sen, T., Della Corte, C.M., Milutinovic, S., Cardnell, R.J., Diao, L., Ramkumar, K., Gay, C.M., Stewart, C.A., Fan, Y., Shen, L., et al. (2019). Combination Treatment of the Oral CHK1 Inhibitor, SRA737, and Low-Dose Gemcitabine Enhances the Effect of Programmed Death Ligand 1 Blockade by Modulating the Immune Microenvironment in SCLC. J. Thorac. Oncol. *14*, 2152–2163. https://doi.org/10.1016/j.jtho.2019.08.009.
14. Sen, T., Tong, P., Stewart, C.A., Cristea, S., Valliani, A., Shames, D.S., Redwood, A.B., Fan, Y.H., Li, L., Glisson, B.S., et al. (2017). CHK1 Inhibition in Small-Cell Lung Cancer Produces Single-Agent Activity in Biomarker-Defined Disease Subsets and Combination Activity with Cisplatin or Olaparib. Cancer Res. *77*, 3870–3884. https://doi.org/10.1158/0008-5472.CAN-16-3409.
15. Taniguchi, H., Caeser, R., Chavan, S.S., Zhan, Y.A., Chow, A., Manoj, P., Uddin, F., Kitai, H., Qu, R., Hayatt, O., et al. (2022). WEE1 inhibition enhances the antitumor immune response to PD-L1 blockade by the concomitant activation of STING and STAT1 pathways in SCLC. Cell Rep. *39*, 110814. https://doi.org/10.1016/j.celrep.2022.110814.
16. Yue, X., Bai, C., Xie, D., Ma, T., and Zhou, P.K. (2020). DNA-PKcs: A Multi-Faceted Player in DNA Damage Response. Front. Genet. *11*, 607428. https://doi.org/10.3389/fgene.2020.607428.
17. Gordhandas, S.B., Manning-Geist, B., Henson, C., Iyer, G., Gardner, G.J., Sonoda, Y., Moore, K.N., Aghajanian, C., Chui, M.H., and Grisham, R.N. (2022). Pre-clinical activity of the oral DNA-PK inhibitor, peposertib (M3814), combined with radiation in xenograft models of cervical cancer. Sci. Rep. *12*, 974. https://doi.org/10.1038/s41598-021-04618-5.
18. Damia, G. (2020). Targeting DNA-PK in cancer. Mutat. Res. *821*, 111692. https://doi.org/10.1016/j.mrfmmm.2020.111692.
19. Burleigh, K., Maltbaek, J.H., Cambier, S., Green, R., Gale, M., James, R.C., and Stetson, D.B. (2020). Human DNA-PK activates a STING-independent DNA sensing pathway. Sci. Immunol. *5*, eaba4219. https://doi.org/10.1126/sciimmunol.aba4219.
20. Hristova, D.B., Oliveira, M., Wagner, E., Melcher, A., Harrington, K.J., Belot, A., and Ferguson, B.J. (2024). DNA-PKcs is required for cGAS/STING-dependent viral DNA sensing in human cells. iScience *27*, 108760. https://doi.org/10.1016/j.isci.2023.108760.
21. Della Corte, C.M., Sen, T., Gay, C.M., Ramkumar, K., Diao, L., Cardnell, R.J., Rodriguez, B.L., Stewart, C.A., Papadimitrakopoulou, V.A., Gibson, L., et al. (2020). STING Pathway Expression Identifies NSCLC With an Immune-Responsive Phenotype. J. Thorac. Oncol. *15*, 777–791. https://doi.org/10.1016/j.jtho.2020.01.009.
22. De Rosa, C., Iommelli, F., Rosa, V.D., Ercolano, G., Sodano, F., Tuccillo, C., Amato, L., Tirino, V., Ariano, A., Cimmino, F., et al. (2024). PBMCs as Tool for Identification of Novel Immunotherapy Biomarkers in Lung Cancer (MDPI).
23. Xiao, R., and Zhang, A. (2022). Involvement of the STING signaling in COVID-19. Front. Immunol. *13*, 1006395. https://doi.org/10.3389/fimmu.2022.1006395.
24. Sharma, A., Kontodimas, K., and Bosmann, M. (2021). The MAVS Immune Recognition Pathway in Viral Infection and Sepsis. Antioxidants Redox Signal. *35*, 1376–1392. https://doi.org/10.1089/ars.2021.0167.
25. Jiang, Z., Wei, F., Zhang, Y., Wang, T., Gao, W., Yu, S., Sun, H., Pu, J., Sun, Y., Wang, M., et al. (2021). IFI16 directly senses viral RNA and enhances RIG-I transcription and activation to restrict influenza virus infection. Nat. Microbiol. *6*, 932–945. https://doi.org/10.1038/s41564-021-00907-x.
26. George, J., Lim, J.S., Jang, S.J., Cun, Y., Ozretić, L., Kong, G., Leenders, F., Lu, X., Fernández-Cuesta, L., Bosco, G., et al. (2015). Comprehensive genomic profiles of small cell lung cancer. Nature *524*, 47–53. https://doi.org/10.1038/nature14664.
27. Ruiz-Fernández de Córdoba, B., Martínez-Monge, R., and Lecanda, F. (2023). ENPP1 Immunobiology as a Therapeutic Target. Clin. Cancer Res. *29*, 2184–2193. https://doi.org/10.1158/1078-0432.CCR-22-1681.
28. Hou, F., Sun, L., Zheng, H., Skaug, B., Jiang, Q.X., and Chen, Z.J. (2011). MAVS forms functional prion-like aggregates to activate and propagate antiviral innate immune response. Cell *146*, 448–461. https://doi.org/10.1016/j.cell.2011.06.041.
29. Sun, Q., Sun, L., Liu, H.H., Chen, X., Seth, R.B., Forman, J., and Chen, Z.J. (2006). The specific and essential role of MAVS in antiviral innate immune responses. Immunity *24*, 633–642. https://doi.org/10.1016/j.immuni.2006.04.004.
30. Cucchi, D., Gibson, A., and Martin, S.A. (2021). The emerging relationship between metabolism and DNA repair. Cell Cycle *20*, 943–959. https://doi.org/10.1080/15384101.2021.1912889.
31. Bian, X., Wang, X., Zhang, Q., Ma, L., Cao, G., Xu, A., Han, J., Huang, J., and Lin, W. (2020). The. Front. Oncol. *10*, 565820. https://doi.org/10.3389/fonc.2020.565820.
32. Park, J.E., Kim, S.E., Keam, B., Park, H.R., Kim, S., Kim, M., Kim, T.M., Doh, J., Kim, D.W., and Heo, D.S. (2020). Anti-tumor effects of NK cells and anti-PD-L1 antibody with antibody-dependent cellular cytotoxicity in

PD-L1-positive cancer cell lines. J. Immunother. Cancer *8*, e000873. https://doi.org/10.1136/jitc-2020-000873.

33. Della Corte, C.M., Barra, G., Ciaramella, V., Di Liello, R., Vicidomini, G., Zappavigna, S., Luce, A., Abate, M., Fiorelli, A., Caraglia, M., et al. (2019). Antitumor activity of dual blockade of PD-L1 and MEK in NSCLC patients derived three-dimensional spheroid cultures. J. Exp. Clin. Cancer Res. *38*, 253. https://doi.org/10.1186/s13046-019-1257-1.
34. Mantovani, A., Sozzani, S., Locati, M., Allavena, P., and Sica, A. (2002). Macrophage polarization: tumor-associated macrophages as a paradigm for polarized M2 mononuclear phagocytes. Trends Immunol. *23*, 549–555. https://doi.org/10.1016/s1471-4906(02)02302-5.
35. Courau, T., Bonnereau, J., Chicoteau, J., Bottois, H., Remark, R., Assante Miranda, L., Toubert, A., Blery, M., Aparicio, T., Allez, M., and Le Bourhis, L. (2019). Cocultures of human colorectal tumor spheroids with immune cells reveal the therapeutic potential of MICA/B and NKG2A targeting for cancer treatment. J. Immunother. Cancer *7*, 74. https://doi.org/10.1186/s40425-019-0553-9.
36. Sutherland, K.D., Ireland, A.S., and Oliver, T.G. (2022). Killing SCLC: insights into how to target a shapeshifting tumor. Genes Dev. *36*, 241–258. https://doi.org/10.1101/gad.349359.122.
37. Lasala, R. (2021). [EMA approval procedures and assessment of innovation by AIFA: a cross sectional analysis]. Recent. Progress. Med. *112*, 273–284. https://doi.org/10.1701/3584.35686.
38. Amouzegar, A., Chelvanambi, M., Filderman, J.N., Storkus, W.J., and Luke, J.J. (2021). STING Agonists as Cancer Therapeutics. Cancers *13*, 2695. https://doi.org/10.3390/cancers13112695.
39. Tong, J., Song, J., Zhang, W., Zhai, J., Guan, Q., Wang, H., Liu, G., and Zheng, C. (2024). When DNA-damage responses meet innate and adaptive immunity. Cell. Mol. Life Sci. *81*, 185. https://doi.org/10.1007/s00018-024-05214-2.
40. Chabanon, R.M., Rouanne, M., Lord, C.J., Soria, J.C., Pasero, P., and Postel-Vinay, S. (2021). Targeting the DNA damage response in immuno-oncology: developments and opportunities. Nat. Rev. Cancer *21*, 701–717. https://doi.org/10.1038/s41568-021-00386-6.
41. Barros, E.M., McIntosh, S.A., and Savage, K.I. (2022). The DNA damage induced immune response: Implications for cancer therapy. DNA Repair *120*, 103409. https://doi.org/10.1016/j.dnarep.2022.103409.
42. Wang, Y., Duan, M., Peng, Z., Fan, R., He, Y., Zhang, H., Xiong, W., and Jiang, W. (2022). Advances of DNA Damage Repair-Related Drugs and Combination With Immunotherapy in Tumor Treatment. Front. Immunol. *13*, 854730. https://doi.org/10.3389/fimmu.2022.854730.
43. Zhang, W., Girard, L., Zhang, Y.A., Haruki, T., Papari-Zareei, M., Stastny, V., Ghayee, H.K., Pacak, K., Oliver, T.G., Minna, J.D., and Gazdar, A.F. (2018). Small cell lung cancer tumors and preclinical models display heterogeneity of neuroendocrine phenotypes. Transl. Lung Cancer Res. *7*, 32–49. https://doi.org/10.21037/tlcr.2018.02.02.
44. Baine, M.K., Hsieh, M.S., Lai, W.V., Egger, J.V., Jungbluth, A.A., Daneshbod, Y., Beras, A., Spencer, R., Lopardo, J., Bodd, F., et al. (2020). SCLC Subtypes Defined by ASCL1, NEUROD1, POU2F3, and YAP1: A Comprehensive Immunohistochemical and Histopathologic Characterization. J. Thorac. Oncol. *15*, 1823–1835. https://doi.org/10.1016/j.jtho.2020.09.009.
45. Cai, L., Liu, H., Huang, F., Fujimoto, J., Girard, L., Chen, J., Li, Y., Zhang, Y.A., Deb, D., Stastny, V., et al. (2021). Cell-autonomous immune gene expression is repressed in pulmonary neuroendocrine cells and small cell lung cancer. Commun. Biol. *4*, 314. https://doi.org/10.1038/s42003-021-01842-7.
46. Lamberti, G., Andrini, E., Sisi, M., Federico, A.D., and Ricciuti, B. (2020). Targeting DNA damage response and repair genes to enhance anticancer immunotherapy: rationale and clinical implication. Future Oncol. *16*, 1751–1766. https://doi.org/10.2217/fon-2020-0215.
47. Perez, B., Aljumaily, R., Marron, T.U., Shafique, M.R., Burris, H., Iams, W.T., Chmura, S.J., Luke, J.J., Edenfield, W., Sohal, D., et al. (2024). Phase I study of peposertib and avelumab with or without palliative radiotherapy in patients with advanced solid tumors. ESMO Open *9*, 102217. https://doi.org/10.1016/j.esmoop.2023.102217.
48. Samuels, M., Falkenius, J., Bar-Ad, V., Dunst, J., van Triest, B., Yachnin, J., Rodriguez-Gutierrez, A., Kuipers, M., You, X., Sarholz, B., et al. (2024). A Phase 1 Study of the DNA-PK Inhibitor Peposertib in Combination With Radiation Therapy With or Without Cisplatin in Patients With Advanced Head and Neck Tumors. Int. J. Radiat. Oncol. Biol. Phys. *118*, 743–756. https://doi.org/10.1016/j.ijrobp.2023.09.024.

STAR★METHODS

KEY RESOURCES TABLE

REAGENT or RESOURCE	SOURCE	IDENTIFIER
Antibodies		
Rabbit monoclonal anti-MAVS (D54A9E)	Cell Signaling (Danvers, MA)	Cat#24930; RRID: AB_2798889
Rabbit monoclonal anti-STING (D2P2F)	Cell Signaling (Danvers, MA)	Cat#13647; RRID: AB_2732796
Rabbit monoclonal anti-phospho-DNA-PKcs (Ser2056) (E9J4G)	Cell Signaling (Danvers, MA)	Cat#68716; RRID: AB_2939025
Rabbit monoclonal anti-DNA-PKcs (E6U3A)	Cell Signaling (Danvers, MA)	Cat#38168; RRID: AB_2799128
Rabbit monoclonal anti-IFI16 (D8B5T)	Cell Signaling (Danvers, MA)	Cat#14970; RRID: AB_2798669
Rabbit monoclonal anti-phospho-TBK1/NAK (Ser172) (D52C2)	Cell Signaling (Danvers, MA)	Cat#5483; RRID: AB_10693472
Rabbit monoclonal anti-TBK1/NAK (E8I3G)	Cell Signaling (Danvers, MA)	Cat#38066; RRID: AB_2827657
Rabbit monoclonal anti-phospho-IRF-3 (Ser386) (E7J8G)	Cell Signaling (Danvers, MA)	Cat#37829; RRID: AB_2799121
Rabbit monoclonal anti-cGAS (D1D3G)	Cell Signaling (Danvers, MA)	Cat#15102; RRID: AB_2732795
Rabbit monoclonal anti-PD-L1 (E1L3N)	Cell Signaling (Danvers, MA)	Cat#13684; RRID: AB_2687655
Rabbit monoclonal anti-Caspase-7	Cell Signaling (Danvers, MA)	Cat#9492; RRID: AB_2228313
Rabbit monoclonal anti-Phospho-Chk1 (Ser345) (133D3)	Cell Signaling (Danvers, MA)	Cat#2348; RRID: AB_331212
Mouse monoclonal anti-Chk1 (2G1D5)	Cell Signaling (Danvers, MA)	Cat#2360; RRID: AB_2080320
Rabbit monoclonal anti-Phospho-Chk2 (Thr68) (C13C1)	Cell Signaling (Danvers, MA)	Cat#2197; RRID: AB_2080501
Rabbit monoclonal anti-Chk2	Cell Signaling (Danvers, MA)	Cat#2662; RRID: AB_2080793
Rabbit monoclonal anti-Phospho-Histone H2A.X (Ser139) (20E3)	Cell Signaling (Danvers, MA)	Cat#9718; RRID: AB_2118009
Rabbit monoclonal anti-Histone H2A.X	Cell Signaling (Danvers, MA)	Cat#2595; RRID: AB_10694556
Mouse monoclonal anti-β-actin (8H10D10)	Cell Signaling (Danvers, MA)	Cat#3700; RRID: AB_2242334
Rabbit monoclonal anti-GAPDH (14C10)	Cell Signaling (Danvers, MA)	Cat#2118; RRID: AB_561053
Mouse monoclonal anti-α-Tubulin	Sigma Chemical Co	Cat#T8203; RRID: AB_1841230
Dynabeads™ Human T-Activator CD3/CD28 for T Cell Expansion and Activation	Gibco	Cat#11131D
Alexa Fluor® 647 Conjugate anti-mouse IgG antibodies	Cell Signaling (Danvers, MA)	Cat#4410; RRID: AB_1904023
Alexa Fluor 488-conjugated anti-rabbit IgG antibodies	Jackson ImmunoResearch Laboratories	Cat# 711-546-152; RRID: AB_2340619
ER-Tracker™ Blue-White DPX	Invitrogen™	Cat# E12353
MitoTracker® Red CMXRos	Cell Signaling Technology	Cat#9082
V500 Mouse Anti-Human CD3	BD Horizon™	Cat#561417; RRID: AB_10611584
FITC Mouse Anti-Human CD45	BD Pharmingen™	Cat#561865; RRID: AB_10896120
PE Mouse Anti-Human CD326 (EpCAM)	BD Pharmingen™	Cat#566841; RRID: AB_2869898
DAPI (4′,6-diamidino-2-phenylindole)	ThermoFisher Scientific	Cat# D1306
Biological samples		
NCI-H524	ATCC	Cat#CRL-5831; RRID:CVCL_1568
DMS79	ATCC	Cat#CRL-2049; RRID: CVCL_1178
NCI-H82	ATCC	Cat#HTB-175; RRID: CVCL_1591
NCI-H209	ATCC	Cat#HTB-172; RRID: CVCL_1525
NCI-H446	ATCC	Cat#HTB-171; RRID: CVCL_1562
NCI-H196	ATCC	Cat#CRL-5823; RRID:CVCL_1509

(*Continued on next page*)

Continued

REAGENT or RESOURCE	SOURCE	IDENTIFIER
NCI-H661	ATCC	Cat#HTB-183; RRID: CVCL_1577
NCI-H1048	ATCC	Cat#CRL-5853; RRID: CVCL_1453
NCI-H2141	ATCC	Cat# CRL-5927; RRID: CVCL_1534
NCI-H1672	ATCC	ATCC Cat#CRL-5886; RRID: CVCL_1486
NCI-H1882	ATCC	Cat# CRL-5903; RRID: CVCL_1504
Human peripheral blood mononuclear cells (PBMCs)	This paper	N/A
Human malignant pleural effusion cells (MPE)	This paper	N/A
Chemicals, peptides, and recombinant proteins		
Recombinant human IL-2 (interleukin 2)	Miltenyi Biotec	Cat#130-097-743
Enpp-1-IN-1 (UUN28589, MV 658), ENPP1 inhibitor	Selleck Chemicals	Cat#S0501
Nedisertib (M3814, Peposertib, MSC2490484A), DNA-PK inhibitor	Selleck Chemicals	Cat#S8586
VX-803 (M4344, ATR inhibitor 2), an ATR inhibitor	Selleck Chemicals	Cat#S9639
Lartesertib (M4076), an ATM inhibitor	Selleck Chemicals	Cat#E1057
Cisplatin (NSC 119875, Cisplatinum, cis-diamminedichloroplatinum II, CDDP, cis DDP, DDP)	Selleck Chemicals	Cat#S1166
Atezolizumab (anti-PD-L1)	Selleck Chemicals	Cat#A2004
Olaparib (AZD2281, KU0059436), a PARP1/2 inhibitor	Selleck Chemicals	Cat#S1060
Protein A/G Plus-Agarose	Santa Cruz Biotechnology	Cat#sc-2001
Critical commercial assays		
Seahorse XF Glycolytic Rate Assay Kit	Agilent	Cat#103344-100
MTS Assay Kit (Cell Proliferation) (Colorimetric)	Abcam	Cat#ab197010
CyQUANT™ LDH Cytotoxicity Assay	Thermo Fisher Scientific, Invitrogen™	Cat#C20300
SensiFAST SYBR Hi-ROX Kit	Meridian Bioscience	Cat#BIO-92005
SensiFAST cDNA Synthesis Kit	Meridian Bioscience	Cat#BIO-65053
Oligonucleotides		
RT-PCR Primers for *STING, cGAS, MAVS, IFI16, PDL-1, FOXP3, TNFα, CXCL10, IL6, IL10, IL4, CCL22, DNAPK* (see Table S1)	OriGene	N/A
MAVS-targeted siRNA	Silencer®, Thermo Fisher	RefSeq. NM_001206491.1
control non-targeting siRNA	Dharmacon Inc.	Cat. D-001810-01-05
ON-TARGETplus Human TMEM173 (340061) siRNA	SMARTpool, Dharmacon	HGNC:27962
ON-TARGETplus Human MB21D1 (115004) siRNA	SMARTpool, Dharmacon	HGNC:21367
Deposited data		
RNA-seq data	This paper	SRA database: PRJNA1208015
SCLC tumor trancriptomic data	George et al. (2015)	EGA database: EGAS00001000925
Software and algorithms		
ImageJ	Schneider et al.	https://imagej.net/ij/download.html
Prism 8	GraphPad Software	https://www.graphpad.com/
BioRender platform	BioRender	https://www.biorender.com/
FACS Diva Software	BD Biosciences	https://www.bdbiosciences.com/en-us/products/software/instrument-software/bd-facsdiva-software

(*Continued on next page*)

Continued

REAGENT or RESOURCE	SOURCE	IDENTIFIER
Wave Desktop 2.6 software	Agilent	https://www.agilent.com/en/product/cell-analysis/real-time-cell-metabolic-analysis/xf-software/seahorse-wave-desktop-software-740897
JAVA GSEA 3.0	GSEA/MSigDB	https://github.com/GSEA-MSigDB/gsea-desktop.git
R version 3.3.0	R Foundation for Statistical Computing	http://www.r-project.org/
Image Lab 3.0.1	BioRad	https://www.bio-rad.com/it-it/product/image-lab-software?ID=KRE6P5E8Z
Other		
BD FACSCanto II	BD Biosciences	N/A
M200 Infinite Pro	Tecan Trading AG	N/A
Seahorse XF96 instrument	Agilent	N/A
APOTOME microscope	ZEISS	N/A
Confocal Airy Scan 2	ZEISS	LSM980
ChemiDoc	BioRad	N/A
QuantStudio 7-Flex	Applied Biosystems	N/A
NanoDrop 2000 spectrophotometer	Thermo Fisher Scientific	N/A

EXPERIMENTAL MODEL AND STUDY PARTICIPANT DETAILS

Study approval

After written informed consent was obtained from patients diagnosed with ES-SCLC, human samples were collected in accordance with the Declaration of Helsinki. The protocol for the use of these samples for research purposes was approved by the Ethics Committee of the University of Campania (“Luigi Vanvitelli”) and Naples (No. 280 on May 16, 2020).

Sample size estimation

We enrolled patients (n=25) with a diagnosis of SCLC receiving one of the following treatments: chemotherapy (cisplatin) and/or an anti-PD-L1 antibody (atezolizumab, durvalumab) as per standard clinical practice. The patients ages ranged from 48 to 87 years (median = 65.7 years) and gender breakdown was 28.7% female and 71.3% male.

How subjects/samples were allocated to experimental groups

The patients were grouped as follows: naïve patients (blood collected at baseline), post-cisplatin patients (blood collected at third day of treatment) and under treatment patients (blood collected after at least two cycles of chemo-immunotherapy treatment). For one SCLC patient (age 65 years old, male) undergoing maintenance therapy with anti-PD-L1 atezolizumab, we collected MPE samples for *ex-vivo* cell line generation.

General informations on partecipants

Detailed patient demographic and clinical characteristics are displayed in Table 1.

Cell lines

The SCLC cell lines NCI-H524 (ATCC Cat#CRL-5831; RRID:CVCL_1568), NCI-DMS79 (ATCC Cat#CRL-2049; RRID: CVCL_1178), NCI-H82 (ATCC Cat#HTB-175; RRID: CVCL_1591), NCI-H209 (ATCC Cat#HTB-172; RRID: CVCL_1525), NCI-H446 (ATCC Cat#HTB-171; RRID: CVCL_1562), NCI-H196 (ATCC Cat#CRL-5823; RRID:CVCL_1509) and NCI-H661 (ATCC Cat#HTB-183; RRID: CVCL_1577) were maintained in RPMI 1640 (Sigma-Aldrich, R8758) supplemented with 10% FBS (Sigma-Aldrich) and 1X penicillin–streptomycin (Sigma-Aldrich, P0781) in a humidity-controlled environment (37°C, 5% CO_2). NCI-H1048 (ATCC Cat#CRL-5853; RRID: CVCL_1453), NCI-H2141 (ATCC Cat# CRL-5927; RRID: CVCL_1534), NCI-H1672 (ATCC Cat#CRL-5886; RRID: CVCL_1486) and NCI-H1882 (ATCC CAT# CRL-5903; RRID: CVCL_1504) cell lines were maintained in HITES medium supplemented with 5% FBS in a humidity-controlled environment (37°C, 5% CO_2). Cell lines were obtained from and authenticated by the American Type Culture Collection (ATCC). Cell lines morphology was monitored, and the cell lines were routinely tested for mycoplasma using a mycoplasma detection kit (InvivoGen).

METHOD DETAILS

Peripheral blood mononuclear cells (PBMCs) isolation

Blood samples were collected in 8.5 ml EDTA tubes from patients with SCLC. PBMCs from patients with SCLC were isolated using lymphosep (Aurogene). Monocytes were mechanically isolated by adherence, and lymphocytes were separated by suspension. Suspension- or adhesion-isolated immune cells were grown for five days in complete medium supplemented with RPMI 1640 containing human autologous serum (10%), ultraglutamine I (1%), penicillin, and streptomycin (1%). Suspension-isolated immune cells were activated with beads coated with anti-CD3 and anti-CD28 (Life Technologies) at a ratio of 1 bead per 10 cells, and IL-2 (Miltenyi Biotech) at a concentration of 20 U/ml. After 24 h, DNA-PKi and/or ENPP1i at 2 μM were added for an additional 72 h.

Reagents

Primary antibodies for western blot analysis against MAVS (D54A9E) (24930, 1:1000), STING (D2P2F) (13647, 1:1000), phospho-DNA-PKcs (Ser2056) (E9J4G) (68716, 1:1000), DNA-PKcs (E6U3A) (38168, 1:1000), IFI16 (D8B5T) (14970, 1:1000), phospho-TBK1/NAK (Ser172) (D52C2) (5483, 1:1000), TBK1/NAK (E8I3G) (38066, 1:1000), phospho-IRF-3 (Ser386) (E7J8G) (37829, 1:1000), cGAS (D1D3G) (15102, 1:1000), PD-L1 (E1L3N) (13684, 1:1000), Caspase-7 (9492, 1:1000), Phospho-Chk1 (Ser345) (133D3) (2348, 1:1000), Chk1 (2G1D5) (2360, 1:1000), Phospho-Chk2 (Thr68) (C13C1) (2197, 1:1000), Chk2 (2662, 1:1000), Phospho-Histone H2A.X (Ser139) (20E3) (9718, 1:1000), Histone H2A.X (2595), β-actin (8H10D10) (3700, 1:2000), GAPDH (14C10) (2118, 1:1000), were purchased from Cell Signaling (Danvers, MA), and α-Tubulin (AA13, 1:2000) was purchased from Sigma Chemical Co. Enpp-1-IN-1, Nedisertib (Peposertib, M3814), VX-803 (M4344), M4076, cisplatin, and atezolizumab were purchased from Selleck Chemicals (Houston, TX).

RNA-sequencing analysis

SCLC cell lines (namely H82, H196, H524, DMS79, H2141, H1672) and PBMCs collected from SCLC patients under treatment (n = 6) were cultured in 6 well plates in appropriate culture medium for 24 h, prior to treatment with cisplatin (0.5 μM) and/or DNA-PKi (2 μM) for 72 h. Cells were harvested and RNA was purified using an RNeasy Plus Mini kit (QIAGEN). The samples were analysed by Novogene Co., Ltd. RNA was evaluated for degradation and contamination and the RNA concentration was assessed. 1 μg of total RNA from each sample was used for library preparation. Messenger RNA was purified from the total RNA using poly-T oligo-attached magnetic beads. After fragmentation, the first strand cDNA was synthesized using random hexamer primers, followed by second strand cDNA synthesis using either dUTP for the directional library or dTTP for the non-directional library. The non-directional library was prepared after end repair, A-tailing, adapter ligation, size selection, amplification, and purification. The directional library was prepared after end repair, A-tailing, adapter ligation, size selection, USER enzyme digestion, amplification, and purification. The library was checked with Qubit and real-time PCR for quantification and a bioanalyzer for size distribution detection. Quantified libraries were pooled and sequenced on an Illumina platform (NovaSeq X Plus Series PE150) according to the effective library concentration and data amount. Raw data in FASTQ format were first cleaned using fastp. Clean data (clean reads) were obtained by removing reads containing adapters, poly-N and low-quality reads from raw data. The reference genome hg38 from the NCBI website was used, and paired-end cleaned reads of the samples were mapped. The index of the reference genome was built using Hisat2 v2.0.5 and paired-end clean reads were aligned to the reference genome using Hisat2 v2.0.5. The mapped reads of each sample were assembled by StringTie (v1.3.3b) in a reference-based approach. Read counts were performed using FeatureCounts v1.5.0-p3, and differential expression analysis was performed using R with the DESeq2 package (v1.20.0). The resulting P-values were adjusted using Benjamini and Hochberg's approach for controlling the false discovery rate. Genes with an adjusted P-value <=0.05 found by DESeq2 were assigned as differentially expressed. GSEA analysis was performed using JAVA GSEA 3.0. All processed RNA-Seq data for SCLC patients-derived PBMCs generated in this study are included in Table S2. All processed RNA-Seq data for SCLC cell lines generated in this study are included in Table S3.

Gene expression

Gene expression data included publicly available data for SCLC tumors (George et al., 2015).[26] Tumor gene expression data is available via the European Genome-phenome Archive under the accession code EGAS00001000925.

RNA extraction and cDNA synthesis

Total RNA was obtained from the cell lines using TRIsure reagent (Meridian Bioscience, BIO-38033). The RNA concentration was measured using a NanoDrop 2000 spectrophotometer (Thermo Fisher Scientific). After RNA extraction, cDNA was generated from 500 ng total RNA using the SensiFAST cDNA Synthesis Kit (Meridian Bioscience, BIO-65053) under the following conditions: 25°C for 10 min, 42°C for 15 min, and 85°C for 5 min.

Gene expression analysis by quantitative reverse transcription-polymerase chain reaction (qRT-PCR)

mRNA expression levels of *STING, MAVS, IFI16, cGAS, PD-L1, CXCL10, TNFα, IL6, IL10, IL4, CCL22 and DNAPK* genes were evaluated by qRT-PCR with a QuantStudio 7-Flex (Applied Biosystems) using the SensiFAST SYBR Hi-ROX Kit (Meridian Bioscience, BIO-92005) under the following conditions: 50°C for 2 min (stage 1), followed by a denaturation step at 95°C for 10 min (stage 2),

followed by 40 cycles at 95°C for 15 s and 60°C for 1 min (stage 3). All samples were run in duplicate, in 20 μL reactions and relative gene expression was determined by normalization to *18S*, which was used as an internal control gene. The 2-ΔCt or 2-ΔΔCt method was used to calculate the relative gene expression. Nonspecific signals caused by primer dimers were excluded by dissociation curve analysis and the use of non-template controls (see Table S1 for primer sequences).

Western blot analysis

Protein lysates from SCLC cells and PBMCs were obtained by homogenization in RIPA lysis buffer [0.1% sodium dodecyl sulfate (SDS), 0.5% deoxycholate, 1% Nonidet, 100 mmol/L NaCl, 10 mmol/L Tris–HCl (pH 7.4), 0.5 mmol/L dithiothreitol, 0.5% phenylmethyl sulfonyl fluoride, protease inhibitor cocktail (Hoffmann-La Roche), and phosphatase inhibitor tablets (PhosSTOP; Roche Diagnostics)] and clarified by centrifugation at 15,000 rpm for 20 min at 4°C. Protein samples containing comparable amounts of proteins, estimated by a modified Bradford assay (Bio-Rad), were resolved by sodium dodecyl sulfate-polyacrylamide gel electrophoresis (SDS-PAGE) and electrotransferred onto 0.2 μm nitrocellulose membranes (Trans-Blot Turbo; Bio-Rad). After blocking the membranes for 90 min at room temperature, they were incubated overnight at 4°C with primary antibodies, followed by incubation with a secondary antibody for 1 h at room temperature. Horseradish peroxidase-conjugated anti-rabbit (Bio-Rad) and anti-mouse (Bio-Rad) antibodies were used as the secondary antibodies. Proteins were detected with Clarity Western ECL Substrate using a ChemiDoc (Bio-Rad). Images were analyzed using Image Lab 3.0.1. Original western blot images are available in this paper's supplemental information (Data S1-S12).

Immunoprecipitation

For the immunoprecipitation (IP) assay, proteins from cell lysates of SCLC cells or PBMC-derived immune cells (250–500 μg) were incubated for 2 h at 4°C with an anti-MAVS rabbit polyclonal antibody (Cell Signaling Technology, 1:50). Then, Protein A/G Plus-Agarose (Santa Cruz Biotechnology, CA, USA) was added to the protein-antibody complexes, which were incubated with shaking overnight at 4°C. The samples were then centrifuged at 12,000 rpm for 5 min. The supernatant was collected and used as the "unbound fraction." The "immunoprecipitated fraction" was washed three times with phosphate-buffered saline (PBS). Proteins were eluted from Protein A/G Plus-Agarose, suspended in SDS buffer, and boiled at 100°C for 5 min before western blotting.

Immunofluorescence

Cells (500.000/well) in 12-well plates were treated with DNA-PKi (2 μM), cisplatin (0.5 μM), and/or ENPP1i (2 μM) for 72 h. Before starting the protocol, 200 nM MitoTracker Deep Red (Cell Signaling Technology) and/or ER-Tracker (Cell Signaling Technology) were added to the culture medium for 45 min. The cells were then fixed for 20 min with a 4% paraformaldehyde (PFA) solution and permeabilized for 10 min with 0.1% Triton X-100 in phosphate-buffered saline (PBS) at room temperature. The cells were then incubated with a specific mouse monoclonal antibody against STING, MAVS, p-IRF3 and DNA-PK in blocking solution (3% BSA in TBS-Tween 0.1%, Sigma) for 2 h at 37°C followed by incubation with Alexa Fluor 488-conjugated anti-rabbit IgG antibodies (Jackson ImmunoResearch Laboratories, West Grove, PA, USA) or Alexa Fluor 647-conjugated anti-mouse IgG antibodies (Jackson ImmunoResearch Laboratories, West Grove, PA, USA) at a dilution of 1: 1000 for 1 h. The nuclei were stained with DAPI (1 μg/mL) (Sigma). Fluorescence was analyzed using an APOTOME microscope. The subcellular localization was assessed using a confocal microscope (Airy Scan 2, ZEISS, LSM980). The relative mean fluorescence intensity (MFI) was analyzed using the ImageJ software (NIH, Bethesda, MD, USA).

Cell energy phenotype and glycolytic rate assay

A Seahorse XF96 instrument (Agilent) was used for the Glycolytic Rate Assay. Prior to the experiment, suspension-isolated immune cells were treated for 72 h with DNA-PKi or ENPP1i. On the day of the experiment, the treated cells were washed and seeded at a density of $5x10^4$ cells/well in 96-well plates coated with Cell-Tak (Corning). The plate was centrifuged to facilitate cell attachment and was incubated at 37°C for 60 min. Glycolytic Rate Assay was performed according to the manufacturer's instructions. Data analysis was performed using Wave Desktop 2.6 software (Agilent).

RNA interference

MAVS-targeted siRNA (Silencer®, Thermo Fisher), ON-TARGETplus Human TMEM173 siRNA (340061, SMARTpool), ON-TARGETplus Human MB21D1 siRNA (115004, SMARTpool) and control non-targeting siRNA (Dharmacon Inc.) were used according to the manufacturer's instructions. Briefly, cell suspension was plated at 40% confluence and allowed to grow in a humidified incubator in 5% CO_2 at 37°C for 24 h. Cells were then transfected with 100 nmol/L siRNAs using Dharmafect reagent (Dharmacon). After 24 h, cells were treated with DNA-PKi or ENPP1i 2 μM for 72 h. After 72 h, cells were recovered and then lysed for western blot analysis. Three independent experiments were performed.

MTS assay

After culturing with adhesion-isolated monocytes, SCLC cells were plated in a 96-well plate (~3,000 cells per well) in serum-free medium, and 3-(4,5-dimethylthiazol-2-yl)-5 -(3-carboxymethoxyphenyl)-2-(4-sulfophenyl)-2H-tetrazolium (MTS; Abcam) was added to each well (10 μL/well) and incubated at 37°C for 2 h. Cell viability was determined spectrophotometrically by measuring absorbance

at 490 nm. The data were expressed as the percentage of viable cells, considering untreated control cells as 100%. At least three independent experiments were performed in triplicate.

Lactate dehydrogenase cytotoxicity assay

Cytotoxicity was assessed by measuring the lactate dehydrogenase (LDH) release from cancer cells into the culture medium. The LDH activity in the medium was determined using a commercially available kit (Thermo Fisher Scientific, Waltham, MA, USA). The assay is based on the conversion of lactate to pyruvate in the presence of LDH, with a parallel reduction in nicotinamide adenine dinucleotide. The formation of nicotinamide adenine dinucleotide hydrate from the above reaction resulted in a change in the absorbance at 340 nm. Aliquots of media and warm reagents were mixed in a 96-well plate according to the manufacturer's instructions, and the absorbance at 680 nm and 490 nm was recorded using an M200 Infinite Pro microplate reader (Tecan Trading AG, Switzerland). To determine LDH activity, the differential values of the 680-nm absorbance value (background signal from the instrument) and 490-nm absorbance value were calculated. The percentage of cytotoxicity was calculated according to the following formula:

$$\% = \frac{(\text{Experimental Value} - \text{Effector Cells Spontaneous Control} - \text{Target Cells Spontaneous Control})}{(\text{Target Cell Maximum Control} - \text{Target Cells Spontaneous Control})}$$

Spheroid formation and 3D coculture protocol

H661, DMS79, or H82 spheroids were generated by seeding 10^4 cells per well in ultralow attachment (Corning) round bottom 6 well plates in complete RPMI. Five days later, cocultures were initiated by adding $5x10^5$ SCLC patients derived suspension-isolated immune cells per well pretreated with DNA-PKi or ENPP1i plus atezolizumab for 72 h before analysis.

Flow cytometry

For flow cytometry, analysis of spheroids and immune cell cocultures, the OUT and IN compartments were isolated by first pooling the 6 coculture wells in 15 ml tubes. The spheroids were gently suspended and left to settle at the bottom of the tube. The supernatant cell suspension consisted of the non-infiltrating immune cells (OUT). These steps were repeated 2 times with PBS to wash spheroids from non-infiltrating immune cells. The spheroids were then disaggregated with Accutase (Merck), suspended in PBS (0.1% BSA) to obtain a single cell suspension (IN), and further analyzed by flow cytometry. At least 500,000 cells were incubated with fluorescently labeled monoclonal antibodies or their respective isotype controls (1/10 diluted 4°C for 30 min in the dark). After washing, the labelled cells were analyzed by flow cytometry using a BD FACSCanto II (Becton Dickinson, Mountain View, CA, USA). The antibodies used were mouse anti-human CD3 V500, mouse anti-human CD45 FITC, and mouse anti-human EpCAM PE (BD Biosciences). The data were analyzed using FACS Diva Software, version 8.0.

Establishment of cell line from Malignant Pleural Effusion of SCLC patient

MPE_1 cell line was established from MPE derived from pathologically proven SCLC patient. MPE samples were directly transferred from the operating room to the laboratory for cell culture. Tumor cells were spun down by centrifugation the MPE sample at 300 rpm for 5 min, and re-suspended with DMEM F12 (GIBCO, CA, USA) supplemented with 10% FBS (Sigma-Aldrich) and 1% Penicillin/Streptomycin (Sigma-Aldrich). Collected cells were then seeded into T-25 cm^2 flasks (Corning, NY, USA). Established cell lines were sustained in RPMI 1640 medium with 10% FBS and 1% (v/v) penicillin and streptomycin (10,000U/ml). Cultures were maintained in humidified incubators at 37°C in an atmosphere of 5% CO_2 and 95% air. The initial passage was assigned when substantial tumor cell growth was detected, and successive passages were given at sub-confluence after trypsinization of the adherent cells. The floating cells were gathered by centrifuging the medium and dispersed by pipetting.

QUANTIFICATION AND STATISTICAL ANALYSIS

The results are expressed as mean ± SEM. Two-group analyses were performed using unpaired t tests. Three or more groups with one independent variable were analyzed using one-way ANOVA. Three or more groups with two independent variables were analyzed using a two-way ANOVA. Statistical analyses were performed using Prism 8 (GraphPad Software, San Diego, CA, USA). All tests were two-tailed, and a P value < 0.05 was considered to indicate statistical significance. Data statistics and bioinformatics analyses for tumor gene expression data were performed using R (https://www.r-project.org/) version R 3.3.0, without the development of original custom codes. Immunoblot analyses, cell viability assays, and quantitative RT-PCR experiments were independently repeated a minimum of three times to ensure reproducibility. Western blotting signals were quantified by morphodensitometric analysis using ImageJ software (NIH, Bethesda, MD, USA). Briefly, the product of the area and optical density of each band was determined and normalized to the same parameter derived from equal loading used. Data are expressed as relative protein levels of each band compared to the corresponding equal loading ± SD. A final graphical summary was drawn in-house using the free BioRender platform.